SorCS1-mediated Sorting of Neurexin in Dendrites Maintains Presynaptic Function

Luís F. Ribeiro[1,2], Ben Verpoort[1,2], Julie Nys[1,2], Kristel M. Vennekens[1,2], Keimpe D. Wierda[1,2] and Joris de Wit[1,2,*]

Affiliations:
[1]VIB Center for Brain & Disease Research, Herestraat 49, B-3000 Leuven, Belgium
[2]KU Leuven, Department of Neurosciences, Leuven Brain Institute, Herestraat 49, B-3000 Leuven, Belgium

[*]**Correspondence**: joris.dewit@kuleuven.vib.be

Abstract

The pre- and postsynaptic membranes comprising the synaptic junction differ in protein composition. The mechanisms that maintain the polarized distribution of synaptic membrane proteins are poorly understood. The sorting receptor SorCS1 is a critical trafficking regulator of neuronal receptors, including neurexin (Nrxn), a presynaptic adhesion molecule essential for synaptic transmission. We find that SorCS1 controls a balance between axonal and dendritic Nrxn1α surface levels. Newly synthesized Nrxn1α traffics to the somatodendritic surface, followed by endocytosis. SorCS1 interacts with the Rab11 effector protein Rab11FIP5/Rip11 to facilitate the transition of internalized Nrxn1α from early to recycling endosomes and bias Nrxn1α surface polarization toward the axon. In the absence of SorCS1, Nrxn1α accumulates in early endosomes and mis-polarizes to the dendritic surface, impairing presynaptic function. The axonal/dendritic balance of Nrxn1α surface distribution is activity-dependent, indicating that SorCS1-mediated sorting in somatodendritic endosomes dynamically controls Nrxn1α axonal surface polarization required for proper presynaptic function.

Introduction

Synapses connect neurons into neural circuits that underlie brain function. Synapses are organized in three major compartments: the presynaptic nerve terminal, the synaptic cleft, and the postsynaptic specialization[1], which differ widely in their protein composition[2,3]. Reliable trafficking mechanisms that control compartment-specific protein composition during formation, maturation, and plasticity of the synapse are thus of key importance for assembly and function of neural circuits[4–6].

Vacuolar protein sorting 10 (VSP10P)-receptor family proteins have emerged as important regulators of intracellular trafficking of numerous ligands in neurons[7,8]. The SorCS1-3 (Sortilin-related CNS expressed) members of the VSP10P family are predominantly expressed in the vertebrate nervous system and regulate the intracellular trafficking of key synaptic surface proteins, including glutamate receptors, neurotrophin receptors, and adhesion molecules[9–13]. These studies identify SorCS proteins as critical regulators of synaptic function and plasticity, but the cellular and molecular mechanisms by which they sort their synaptic cargo proteins remain poorly understood.

SorCS1 is an endosomal sorting receptor that cycles between the plasma membrane and the endosomal pathway[7–9]. A key SorCS1 cargo protein is the synaptic adhesion molecule neurexin (Nrxn). SorCS1 directly binds Nrxn via an extracellular domain *cis* interaction and is required for surface and synaptic localization of Nrxn[13]. Nrxns, in mammals expressed from three genes as α-, β-, and γ-Nrxns, are presynaptic adhesion molecules that engage in a network of interactions with multiple pre- and postsynaptic ligands[14]. Nrxns act in a cell type-specific manner to regulate synapse number and function[15–17]. Mutations in *NRXNs* have been associated with multiple neuropsychiatric disorders, especially schizophrenia and autism[18–20], underscoring the importance of Nrxns for normal brain function. Despite their essential role, little is known about the mechanisms that control presynaptic localization and abundance of Nrxns[21].

Here, we show that the sorting receptor SorCS1 controls a balance between axonal and dendritic Nrxn surface levels. In mature neurons, newly synthesized Nrxn1α traffics to the somatodendritic plasma membrane, followed by endocytosis, endosomal sorting and translocation to the axon via a transcytotic pathway. SorCS1 interacts with the Rab11 effector protein Rab11FIP5/Rip11 to facilitate the transition of internalized Nrxn1α from early to recycling endosomes and bias surface polarization of Nrxn1α toward the

axon. In the absence of SorCS1, Nrxn1α accumulates in early endosomes and mis-polarizes to the dendritic surface, impairing synapse formation and presynaptic function. The balance between the axonal/dendritic surface distribution of Nrxn1α is activity-dependent, indicating that SorCS1-mediated sorting in dendrites maintains the axonally polarized distribution of Nrxn1α that is required for proper presynaptic function.

Results

SorCS1-mediated sorting in dendrites regulates Nrxn1α axonal surface polarization

We first determined the subcellular distribution of endogenous SorCS1 in neurons, which has remained uncertain due to a lack of suitable antibodies for the immunodetection of SorCS1. To this end, we generated a SorCS1 knock-in (KI) mouse (*Sorcs1*$^{HA/HA}$), using CRISPR/Cas9 to insert a hemagglutinin (HA) epitope tag in the *Sorcs1* locus (Supplementary Fig. 1a,b). HA immunodetection in *Sorcs1*$^{HA/HA}$ cortical neurons revealed prominent punctate SorCS1 immunoreactivity in soma and dendrites (Fig. 1a,c), which was mimicked by HA-tagged SorCS1 exogenously expressed in wild-type (WT) hippocampal neurons (Fig. 1b,c). These results show a preferentially somatodendritic distribution for SorCS1, suggesting that SorCS1-mediated sorting of cargo proteins occurs in this compartment.

To investigate the mechanism by which SorCS1 controls the surface distribution of Nrxn, we used primary cultures of cortical neurons, which strongly express *Sorcs1*[22,23], and focused on Nrxn1α as one of the most abundant Nrxn isoforms in the brain[15,24]. Cortical *Sorcs1*$^{flox/flox}$ mouse neurons were electroporated with GFP-tagged Cre recombinase (Cre) to remove SorCS1 (*Sorcs1* KO), transfected with HA-tagged Nrxn1α (HA-Nrxn1α), and live-labeled with an HA antibody in combination with Ankyrin-G and MAP2 immunodetection to analyze the surface distribution of Nrxn1α in the axonal and dendritic compartments, respectively. Loss of SorCS1 caused a decrease in Nrxn1α axonal surface levels and a concomitant increase in dendritic surface levels compared to control cells expressing GFP, changing Nrxn1α surface polarization from axonal to dendritic (Fig. 1d,e). Re-expression of WT SorCS1 (SorCS1^{WT}) in Cre-positive *Sorcs1*$^{flox/flox}$ neurons restored Nrxn1α surface polarization (Fig. 1d,e), indicating that the

defect occurred cell-autonomously. Rescue with the endocytosis-defective mutant[25] of SorCS1 (SorCS1^{Y1132A}), which remains on the plasma membrane (Supplementary Fig. 1c,d), did not rescue Nrxn1α surface polarization (Fig. 1d,e), suggesting that SorCS1 is either required for endocytosis of Nrxn1α or needs to localize to endosomes to regulate the surface balance of Nrxn1α between axon and dendrites. Taken together, these results indicate that SorCS1 acts in the somatodendritic compartment to control a balance between dendritic and axonal surface expression of Nrxn1α and bias Nrxn1α surface polarization toward the axon.

Indirect axonal trafficking of Nrxn1α

Our results suggests that Nrxn1α traffics through both dendritic and axonal compartments. To monitor Nrxn1α trafficking in cortical neurons, we employed the retention using selective hooks (RUSH) system[26] to retain Nrxn1α in the endoplasmic reticulum (ER) and induced synchronous release and transport through the secretory pathway by application of biotin (Fig. 2a). We performed live-cell imaging in 8–10 days in vitro (DIV) rat cortical neurons co-expressing SBP-GFP-Nrxn1α (reporter) and streptavidin-KDEL (ER hook), and live-labeled these with an antibody against the axon initial segment (AIS) protein Neurofascin (Supplementary Fig. 2a) to visualize the axonal compartment.

At t=0, we observed diffuse SBP-GFP-Nrxn1α fluorescence in soma and dendrites, in a pattern resembling the ER (Fig. 2b). Following application of biotin, Nrxn1α fluorescence coalesced into punctate structures that started trafficking abundantly in the somatodendritic compartment, followed by Nrxn1α trafficking in the axon after a marked delay (Fig. 2c; Supplementary Movie 1). Quantification of Nrxn1α fluorescence intensity showed a decrease in Nrxn1α intensity in the soma and an increase in axonal intensity approximately 90 min after biotin application (Fig. 2e). Trafficking of the somatodendritic cargo protein TfR[27] was detected only in the somatodendritic compartment (Fig. 2d,f; Supplementary Movie 2); and in the absence of biotin, dendritic SBP-GFP-Nrxn1α-positive structures were not motile (Supplementary Movie 3), indicating that the delayed trafficking of Nrxn1α to axons is not simply caused by prolonged ER retention. Moreover, immature DIV3 neurons displayed Nrxn1α trafficking to the axonal compartment shortly after biotin application (Supplementary Fig. 2b,c; Supplementary Movie 4), further

indicating that the delayed axonal trafficking of Nrxn1α in mature neurons does not result from prolonged retention in the ER but correlates with the maturation state of the neuron.

To analyze the dynamics of Nrxn1α-positive vesicles in both neuronal compartments, we analyzed vesicle trafficking at early (20–34 min) and late (1–2 hr) time points after Nrxn1α release from the ER. Kymograph analysis showed a small increase in the mean number of vesicles present in dendrites at late compared to early time-points, as a consequence of an increased number of motile vesicles (Fig. 2g,h; Supplementary Movies 5,6). Shortly after ER release, the majority of vesicles in dendrites moved in the anterograde direction, shifting to a retrograde movement at the later time-point (Fig. 2i). Strikingly, motile Nrxn1α vesicles were absent in axons shortly after ER release but increased dramatically at late time-points (Fig. 2j,k; Supplementary Movies 5,6). The vast majority of these vesicles moved anterogradely (Fig. 2l).

In a complementary approach, we transfected mouse cortical neurons with HA-Nrxn1α and treated these with a reversible blocker of anterograde Golgi trafficking (Supplementary Fig. 2e), brefeldin A (BFA)[28], to allow synchronized release of Nrxn1α. Following BFA wash-out and resumption of trafficking, Nrxn1α was first detected on the dendritic surface before appearing on the axonal surface (Supplementary Fig. 2d,f–h). Together, these results show that following transport through the secretory pathway, Nrxn1α is first inserted in the somatodendritic plasma membrane and appears on the axonal surface with a marked delay.

Endocytosis and endosomal transport are required for axonal polarization of Nrxn1α

Our observations suggest an indirect, dendrite-to-axon trafficking route for Nrxn1α. This is reminiscent of the transcytotic trafficking pathway[29], in which cargo is first delivered to the somatodendritic plasma membrane, followed by internalization into endosomes and trafficking to the axonal compartment via endosome-derived carriers. To monitor Nrxn1α intracellular transport, mouse cortical neurons transfected with HA-Nrxn1α were incubated with an anti-HA antibody, washed and returned to the incubator for 15 or 40 min of chase (antibody pulse-chase assay; Supplementary Fig. 3a). Internalized Nrxn1α was largely restricted to the dendritic compartment (Supplementary Fig. 3a,b) and shifted from early endosomes (EEs; EEA1- and Rab5-positive) to recycling endosomes (REs; Rab11-positive) over time (Supplementary Fig.

3c–h). Blocking of dynamin-dependent endocytosis, either by expressing a dominant-negative mutant of Dynamin1 (K44A) (Supplementary Fig. 4a,b) or with Dynasore (Supplementary Fig. 4c,d), caused a decrease in Nrxn1α axonal surface levels and a concomitant increase in dendritic surface levels . Expression of GTP binding-deficient mutants of Rab5 (S34N) and Rab11 (S25N), to interfere with transport to early and recycling endosomes, respectively, mimicked the effect of blocking endocytosis (Supplementary Fig. 4e–h). However, expression of Rab7 (T22N) to interfere with transport to late endosomes did not affect the axonal surface polarization of Nrxn1α (Supplementary Fig. 4i,j). Thus, endocytosis, early and recycling endosomal transport, but not late endosomal transport, are required for accumulation of Nrxn1α on the axonal plasma membrane. Consistent with these observations, neurons transfected with HA-Nrxn1α and chased for 90 min with an anti-HA antibody showed increased levels of internalized Nrxn1α in the axon compared to neurons chased for 15 min (Supplementary Fig. 3i,j). As Nrxn1α endocytosis is largely restricted to the dendritic compartment (Supplementary Fig. 3a,b,i,j), dendritic plasma membrane-derived Nrxn1α is the most likely source for sustaining this increase in internalized Nrxn1α detected in the axon. Taken together, these results indicate that Nrxn1α is trafficked to the axon via the transcytotic route.

SorCS1-mediated sorting controls the subcellular distribution of endogenous Nrxn

Transcytotic trafficking implies that endogenous Nrxns will also localize to dendrites, at least transiently. Several independent studies have reported the presence of a dendritic pool of Nrxn[13,30–33], in addition to axonal localization, but this has remained controversial due to the lack of suitable antibodies for the detection of endogenous Nrxns. To unequivocally determine the subcellular localization of endogenous Nrxn1α in neurons, we generated a Nrxn1α KI mouse (*Nrxn1α*$^{HA/HA}$) (Supplementary Fig. 5a,b). We cultured *Nrxn1α*$^{HA/HA}$ cortical neurons together with WT mouse cortical neurons, such that the majority of presynaptic inputs onto *Nrxn1α*$^{HA/HA}$ neurons are from WT, unlabeled cells, enabling the reliable detection of HA-Nrxn1α in the somatodendritic and axonal compartment (Supplementary Fig. 5c). In permeabilized DIV3 *Nrxn1α*$^{HA/HA}$ neurons, total Nrxn1α localized to a perinuclear compartment and displayed a punctate distribution in dendrites and axons, with prominent accumulation at dendritic tips and axonal growth cones (Fig. 3a). In DIV7 and DIV11 neurons, dendritic localization became more pronounced (Fig. 3a,b;

Supplementary Fig. 5d). Quantification of the axonal/dendritic ratio of the total pool of endogenous Nrxn1α indicated a shift from axonal to dendritic enrichment of Nrxn1α as neurons mature (Fig. 3b). Surface Nrxn1α showed a polarized distribution toward the axon at all developmental time points analyzed (Fig. 3c,d). The localization pattern observed in *Nrxn1α*$^{HA/HA}$ neurons was recapitulated in WT neurons labeled with a pan-Nrxn antibody[34] (Fig. 3e,f), which shows specific labeling of endogenous Nrxn in cultured mouse cortical neurons (Supplementary Fig. 5g,h), or transfected with exogenous HA-Nrxn1α (Supplementary Fig. 5e,f). Thus, endogenous Nrxn1α is an axonally polarized surface protein that accumulates in dendrites as neurons mature.

To test the role of transcytosis in the subcellular distribution of endogenous Nrxn1α, we blocked endocytosis in *Nrxn1α*$^{HA/HA}$ neurons using the K44A Dynamin1 mutant. Expression of K44A-Dynamin1 reduced the axonal intensity of total endogenous Nrxn1α and decreased the balance between axonal and dendritic Nrxn1α levels in *Nrxn1α*$^{HA/HA}$ cortical neurons (Fig. 3g,h), indicating that endocytosis is required for axonal polarization of endogenous Nrxn1α.

To determine whether SorCS1-mediated sorting controls the subcellular distribution of endogenous Nrxn, we immunostained *Sorcs1*$^{flox/flox}$ neurons electroporated with Cre or GFP with the pan-Nrxn antibody. Loss of SorCS1 reduced axonal intensity of total endogenous Nrxn and decreased the axonal/dendritic ratio for endogenous Nrxn compared to control neurons (Fig. 3i,j). Taken together, these findings demonstrate that the axonally polarized distribution of endogenous Nrxn is controlled by transcytosis and SorCS1-mediated sorting.

Selective mis-sorting of transcytotic cargo in the absence of SorCS1

We next determined whether the surface polarization of other axonal membrane proteins was affected in the absence of SorCS1. The cell adhesion molecules L1/NgCAM and Caspr2 are both targeted to the axonal surface, but via distinct trafficking routes. L1/NgCAM is transcytosed from dendrites to axon[35,36]. Caspr2 is indiscriminately delivered to both axon and dendrites but is selectively endocytosed from the somatodendritic surface, resulting in axonal polarization[37]. *Sorcs1*$^{flox/flox}$ cortical neurons electroporated with Cre or GFP were transfected with myc-L1 or HA-Caspr2 and immunostained for surface myc (Supplementary Fig. 6a) or HA (Supplementary Fig. 6b). Consistent with a general role for SorCS1 in

regulating the transcytotic pathway, surface polarization of L1/NgCAM, but not of Caspr2, was perturbed by SorCS1 loss (Supplementary Fig. 6a–c). The polarity index of two somatodendritic proteins (GluA2 and MAP2), was unchanged in *Sorcs1* KO neurons (Supplementary Fig. 7), indicating that loss of SorCS1 does not generally perturb the polarized distribution of neuronal proteins. Together, these results show that loss of SorCS1 selectively impairs the transcytotic route, while keeping other neuronal polarity mechanisms intact.

A SorCS1-Rab11FIP5 interaction controls Nrxn1α transition from early to recycling endosomes

The cellular and molecular mechanisms by which SorCS1 sorts its cargo remain unclear. Our previous SorCS1 interactome analysis[13] identified multiple components of the endocytic machinery associated with SorCS1. To dissect which sorting step of Nrxn1α is disrupted in *Sorcs1* KO neurons, we followed the fate of internalized Nrxn1α throughout the endosomal pathway (Supplementary Fig. 8e).

To determine whether SorCS1 is required for endocytosis of Nrxn1α, we repeated the antibody pulse-chase assay in *Sorcs1*$^{flox/flox}$ cortical neurons. Internalization of HA-Nrxn1α in dendrites after 20 min of chase was not affected in *Sorcs1* KO neurons compared to control cells (Supplementary Fig. 8a,b), indicating that SorCS1 is not required for Nrxn1α endocytosis.

We next analyzed endosomal trafficking of Nrxn1α in *Sorcs1* KO neurons. *Sorcs1*$^{flox/flox}$ mouse cortical neurons expressing Cre and HA-Nrxn1α were chased for 20 (Fig. 4a), 25 (Fig. 4c), 40 (Fig. 4e) and 90 min (Fig. 4g) to analyze the colocalization of internalized Nrxn1α with EEs (EAA1), fast REs (Rab4), REs (Rab11) in dendrites, and REs (Rab11) in the axon, respectively. Quantification revealed an increase in the colocalization of internalized Nrxn1α with EEs and Rab4-fast REs in dendrites of *Sorcs1* KO neurons compared to control neurons (Fig. 4b,d). Colocalization of internalized Nrxn1α with Rab11-REs in *Sorcs1* KO neurons was decreased in dendrites (Fig. 4f) and even more strongly reduced in the axon (Fig. 4h). Thus, in the absence of SorCS1-mediated sorting, Nrxn1α accumulates in EEs and is mis-sorted to Rab4-fast REs. These observations are consistent with our finding that dendritic surface levels of Nrxn1α are increased in *Sorcs1* KO neurons (Fig. 1a,b), which is likely due to increased recycling of Nrxn1α from Rab4-positive endosomes back to the dendritic plasma membrane. Similarly, the reduced axonal surface levels of Nrxn1α (Fig. 1a,b) likely result from decreased sorting of Nrxn1α to Rab11-REs. Together, these

results indicate that SorCS1 plays a critical role in the transition of Nrxn1α from EEs to Rab11-REs (Supplementary Fig. 8e).

We reasoned that SorCS1 interacts with additional proteins to facilitate Nrxn1α sorting from early to recycling endosomes. Rab11 family-interacting protein 5 (Rab11FIP5/Rip11; from here on Rip11), is prominently present in the raw mass spectrometric (MS) data set obtained after affinity purification (AP) of SorCS1 complexes from rat brain extracts with two independent antibodies[13] (AP-MS data available online). Rip11, which belongs to the family of Rab11-interacting proteins[38], localizes to REs in polarized epithelial cells and regulates transcytosis of proteins from the basolateral to the apical plasma membrane[39,40]. A possible role of Rip11 in neuronal transcytosis has not been reported. Western blot analysis of immunoprecipitated HA-SorCS1 from postnatal *Sorcs1*$^{HA/HA}$ KI cortical extracts showed strong HA-SorCS1 enrichment and a robust Rip11 band, which are absent in the mouse IgG control (Fig. 4i), validating the AP-MS data. Like SorCS1, Rip11 predominantly localized to the somatodendritic compartment (Supplementary Fig. 8c,d), where it displayed a punctate distribution and robustly colocalized with SorCS1 (Fig. 4j,k). Expression of a dominant-negative (DN) form of Rip11 that inhibits the transport from early to recycling endosomes[41] reduced axonal surface levels of HA-Nrxn1α and increased dendritic surface levels, shifting Nrxn1α surface polarization from axonal to dendritic (Fig. 4l,m). Together, these results indicate that a SorCS1-Rip11 interaction facilitates sorting of Nrxn1α from early to recycling endosomes, thus biasing trafficking to the axon while preventing mis-sorting to fast recycling and late endosomes (Supplementary Fig. 8e).

Loss of SorCS1 impairs Nrxn-mediated synaptogenesis

Mis-sorting of Nrxn to the dendritic surface in *Sorcs1* KO neurons would be expected to impair synapse formation on heterologous cells expressing a postsynaptic ligand for Nrxn[42,43]. We infected *Sorcs1*$^{flox/flox}$ cortical neurons with lentivirus (LV) to express Cre-T2A-mCherry or mCherry as control and co-cultured these with HEK293T cells expressing FLAG-Neuroligin 1 (Nlgn1). FLAG-Nlgn1 induced strong clustering of the presynaptic marker Synapsin1 in control axons contacting the HEK293T cell surface (Fig. 5a). Loss of SorCS1 reduced Nlgn1-mediated Synapsin1 clustering (Fig. 5a). This defect was specific, as presynaptic differentiation induced by Netrin-G Ligand 3 (NGL-3), which requires leukocyte common

antigen-related protein (LAR) in axons[44], was not affected in *Sorcs1* KO neurons (Fig. 5b). Infection with a lentiviral vector expressing shRNAs against all Nrxns (Nrxn TKD)[42,45] mimicked the defect in *Sorcs1* KO neurons (Fig. 5a), suggesting that Nlgn1-induced presynaptic differentiation is impaired in *Sorcs1* KO neurons due to decreased axonal surface levels of Nrxn. To test this, we expressed Nrxn1α in *Sorcs1* KO neurons using LV. Expression of Nrxn1α, which mis-polarizes to the dendritic surface in *Sorcs1* KO neurons, did not rescue the impaired Nlgn1-mediated synaptogenic activity (Fig. 5a). However, expression of a Nrxn1α deletion mutant lacking the cytoplasmic 4.1-binding motif (Δ4.1), which bypasses the transcytotic route and SorCS1-mediated sorting (Supplementary Fig. 9), rescued the synaptogenic defect caused by SorCS1 loss (Fig. 5a). These results show that SorCS1-mediated sorting of Nrxns, by promoting Nrxn accumulation on the axonal surface, is required for normal synaptogenesis onto Nlgn1-expressing cells.

SorCS1-mediated sorting is required for presynaptic function

In the absence of SorCS1, mis-sorting of Nrxns, which regulate neurotransmitter release[15–17], would be expected to impair presynaptic function. To assess the consequences of loss of SorCS1 on synaptic function, we recorded spontaneous miniature excitatory postsynaptic currents (mEPSCs) from *Sorcs1*$^{flox/flox}$ autaptic cortical cultures electroporated with Cre or GFP. SorCS1 loss strongly decreased mEPSC frequency (Fig. 6a,b). Decay kinetics and amplitude of mEPSCs were not altered by loss of SorCS1 (Fig. 6a,b), suggesting that the amount of neurotransmitter release per vesicle and postsynaptic receptor properties were not affected. The amplitude and total charge transfer of single evoked EPSCs (eEPSCs) were reduced in *Sorcs1* KO neurons (Fig. 6c,d). The mEPSC frequency and eEPSC amplitude defects can be attributed to a decrease in the readily releasable pool (RRP) size or in the vesicular release probability (Pves). To assess these parameters, we applied a hyperosmotic sucrose stimulus. The amplitude and total charge transfer of synaptic responses (Fig. 6e,f) and RRP size (Fig. 6g) induced by single application of 0.5 M sucrose were strongly decreased in *Sorcs1* KO neurons. Because eEPSC amplitude and RRP size were proportionally reduced in *Sorcs1* KO cells, the Pves (evoked EPSC charge/initial sucrose charge) was unchanged (Fig. 6h). To further examine the synaptic defects in *Sorcs1* KO neurons, we performed train stimulations of 20 stimuli at different frequencies to probe for short-term

plasticity defects that cannot be detected by induction of single EPSC and single sucrose application. Repeated stimulation at 10 Hz produced a more pronounced rundown of normalized evoked responses (synaptic depression) in *Sorcs1* KO neurons compared to control cells (Fig. 6i,j). Furthermore, paired-pulse ratio (PPR) measurement at different inter-stimuli intervals further showed the increase in synaptic depression caused by SorCS1 loss (Fig. 6k), suggesting that active excitatory synapses in *Sorcs1* KO cells have reduced neurotransmitter release. Indeed, the RRP size and release kinetics during 10 Hz-train stimulation (Supplementary Fig. 10) calculated by back-extrapolation were reduced in *Sorcs1* KO neurons, indicating a presynaptic defect independent of the silent synapses phenotype that we described previously[13]. Together, these observations indicate that loss of SorCS1 impairs neurotransmitter release, reminiscent of Nrxn loss-of-function[15–17], supporting the notion that SorCS1-mediated transcytosis of Nrxns is required for normal presynaptic function.

The axonal/dendritic balance of Nrxn surface polarization is activity-dependent

Finally, we tested whether the axonal/dendritic balance of Nrxn surface polarization is regulated in response to changes in activity. Cortical cultures were treated either with picrotoxin (PTX) or tetrodotoxin (TTX) for 48 hr. PTX ($GABA_A$ receptor blocker) and TTX (voltage-gated sodium channel blocker) cause global changes in neuronal activity, by increasing or decreasing the neuronal firing rates, inducing homeostatic scaling down or scaling up[46], respectively. PTX treatment led to a loss of exogenous Nrxn1α from the axonal surface, concomitant with an increase on the dendritic surface, changing Nrxn1α surface polarization from axonal to dendritic (Fig. 7a,b). The axonal/dendritic balance of endogenous Nrxns, detected with a pan-Nrxn antibody, was also shifted toward dendritic polarization in PTX-treated neurons (Fig. 7c,d). Conversely, TTX-treated neurons showed an increase in axonal surface polarization of Nrxn1α (Fig. 7e,f). After SorCS1 depletion from cortical neurons, TTX treatment failed to increase the axonal surface polarization of Nrxn1α (Fig. 7g,h). In conclusion, these observations indicate that neurons can dynamically change the axonal/dendritic surface balance of Nrxns in response to bidirectional changes in activity, likely in a SorCS1-mediated transcytosis-dependent manner.

Discussion

The mechanisms by which neurons control the polarized distribution and abundance of key synaptic membrane proteins are poorly understood. Here, we show that SorCS1-mediated sorting in somatodendritic endosomes controls a balance between axonal and dendritic surface levels of Nrxn and dynamically maintains Nrxn axonal surface polarization required for proper presynaptic function.

SorCS1 sorts cargo to the transcytotic pathway

The mechanism by which SorCS1 regulates neuronal cargo trafficking has remained unclear. We find that SorCS1 controls a balance between axonal and dendritic surface polarization of Nrxn. In mature neurons, newly synthesized Nrxn1α traffics to the somatodendritic surface. Following endocytosis, SorCS1 mediates Nrxn1α sorting from early (Rab5-positive) to recycling endosomes (Rab11-positive). Nrxn1α-containing REs are subsequently transcytosed from dendrites to the axon. In agreement, blocking of endocytosis, EE-, and RE-mediated transport all shift the axonal/dendritic surface balance of Nrxn1α toward the dendrite. These effects are mimicked by *Sorcs1* KO. We find that SorCS1 is required for the transition of endocytosed Nrxn1α from EEs to REs and identify the Rab11-interacting protein Rab11FIP5/Rip11 as a novel SorCS1 interactor. Interference with Rip11 function alters the axonal-dendritic surface balance of Nrxn1α in the same way that *Sorcs1* KO does. Rab11FIPs function as linkers between Rab11 and motor proteins to promote sorting of cargo from EEs to REs[38,47] and transcytosis in polarized epithelial cells[39,40], but their function in neuronal transcytosis has not been explored. Our data suggest that SorCS1/Rip11 form a protein complex that localizes to dendritic endosomes and sorts internalized Nrxn1α from early to recycling endosomes, thus biasing the trafficking of Nrxn1α-containing REs to the axon while preventing Nrxn1α mis-sorting to lysosomes and the dendritic surface (Supplementary Fig. 8e).

The transcytotic pathway has been proposed as the canonical mechanism for protein and lipid trafficking across the basolateral and the apical cell membranes and establishment of cell polarity in polarized epithelial cells[48]. In neurons, where the somatodendritic and axonal compartments are thought to be the equivalent of the basolateral and apical domains of polarized epithelial cells[49], respectively, the role of transcytosis is less well-established. In fact, few cargoes (NgCAM/L1[35,36], Trk receptors[50], CB1R[51]

and BACE1[52]) in neurons have been shown to be translocated from dendrites to the axon. We show that SorCS1 loss impairs trafficking of Nrxns and NgCAM, but not of Caspr2, which traffics via the selective endocytosis/retention pathway[37], supporting a role for SorCS1 in regulating the transcytotic pathway in the maintenance of neuronal polarity.

SorCS1-mediated sorting of Nrxn1α in dendrites can be circumvented by deleting the 4.1-binding motif in the cytoplasmic tail of Nrxn1α. It remains to be elucidated whether Nrxn1α's 4.1-binding motif, which lacks canonical YxxØ and [D/E]xxx[L/I] dendritic sorting motifs[53] but contains several tyrosine residues, is required for initial sorting to dendrites or for insertion in the dendritic membrane. Binding of the GluA1 AMPAR subunit to the 4.1N protein is required for membrane insertion[54]. We find that the extracellular domain of Nrxn1α is required for somatodendritic sorting (data not shown), suggesting that deletion of the 4.1-binding motif in Nrxn1α impairs dendritic insertion but not initial sorting to this compartment. Deletion of the 4.1-binding motif in Nrxn1α may further allow axonal sorting motifs present within the 1495–1511 and/or 1516–1527 amino acid stretches of the cytoplasmic domain (Supplementary Fig. 9) to drive axonal targeting of Nrxn1α. Thus, a combination of extracellular and intracellular motifs contributes to the polarized surface distribution of Nrxn1α and likely allows for regulation by signaling pathways.

SorCS1-mediated sorting of Nrxn and synaptic function

Presynaptic differentiation in *Sorcs1* KO axons contacting Nlgn1-expressing HEK293T cells, but not NGL-3-expressing cells, is impaired. Nrxn TKD in neurons mimics this defect, in agreement with previous observations[42]. Expression of the Nrxn1α deletion mutant lacking the 4.1-binding motif in *Sorcs1* KO neurons rescues the defect in presynaptic differentiation on Nlgn1-expressing heterologous cells. Together, these results suggest that the selective impairment in Nlgn1-induced presynaptic differentiation in *Sorcs1* KO neurons is due to a decrease in the abundance of axonal surface Nrxns.

Nrxns play key roles in neurotransmitter release[15–17]. Alpha-Nrxn KO in neocortical cultured slices reduces mEPSC/mIPSC frequency and eIPSC amplitude[17]. Beta-Nrxn KO in cortical neurons decreases mEPSC frequency and eEPSC amplitude[15]. Similarly, loss of SorCS1 in autaptic cortical neurons results in decreased mEPSC frequency and eEPSC amplitude. In addition, loss of SorCS1 in autaptic cortical

neurons decreased the amplitude of sucrose-evoked EPSC and increased the synaptic depression of normalized eEPCSs during stimulus trains, similar to alpha-Nrxn KO neurons[17]. Together, these results suggest that mis-trafficking of Nrxn is a major contributor to the defects in presynaptic function in *Sorcs1* KO neurons. These defects are likely attributed to a decrease in neurotransmitter release, rather than a decrease in excitatory synapse density, which is unaffected in *Sorcs1* KO cortical neurons[13] and in Nrxn TKD hippocampal neurons[42].

A dynamic axonal/dendritic surface balance of Nrxn

Using CRISPR/Cas9-mediated epitope tagging of endogenous Nrxn1α, we demonstrate unequivocally that Nrxn1α is an axonally polarized surface protein with a substantial presence in dendrites. The axonal-dendritic balance of Nrxn1α is developmentally regulated. Early in neuronal development, endogenous Nrxn1α is enriched in the axon and traffics directly to the axon after TGN exit. As neurons mature, Nrxn1α trafficking changes to a dendrite-exclusive insertion after TGN exit, and accumulation of Nrxn1α at the axonal surface is sustained via a SorCS1-dependent transcytotic pathway. The biological function of this developmental regulation and circuitous trafficking route is not clear. One hypothesis that has been put forward is that transcytosis in neurons provides an efficient way of delivering receptors from a reservoir of readily-synthesized proteins. Similar to other transcytotic axonal cargo, a dendritic pool of Nrxn may supply the demand for receptors along the axonal surface, either constitutively[50,51] or in response to ligand-receptor interactions and signalling[50,55]. Supporting this idea, we find that the axonal/dendritic surface balance of Nrxn is activity-dependent. SorCS1-mediated sorting could thus dynamically regulate Nrxn surface distribution to adjust presynaptic release properties in response to signaling and neuronal activity.

Dendritically localized Nrxns might have a function in this compartment. Postsynaptically expressed Nrxn1 decreases Nlgn1's synaptogenic effect in hippocampal neurons, likely by *cis*-inhibition of Nlgn1 that prevents trans-synaptic interaction with presynaptic Nrxns[32]. In retinal ganglion cells, a shift in Nrxn localization away from dendrites has been proposed to allow dendritic innervation[30]. In cortical neurons we observe the opposite: Nrxn surface expression in dendrites increases with maturation. Possibly, dendritic Nrxns modulate the function of postsynaptic Nrxn ligands, such as Nlgns, which control postsynaptic neurotransmitter receptor function[56], or LRRTM1, which shapes presynaptic properties[57].

Consistent with such a modulatory role, loss of alpha-Nrxns in cortical neurons results in a cell-autonomous decrease in NMDA receptor-dependent postsynaptic currents, likely reflecting a change in the postsynaptic localization of NMDA receptors[58]. At the *C. elegans* neuromuscular junction, the ectodomain of postsynaptic Nrxn is proteolytically cleaved and binds to the presynaptic α2δ calcium channel subunit to inhibit presynaptic release[59].

Our observation that critical cargo stalls in EEs in the absence of SorCS1-mediated sorting is reminiscent of the enlarged EEs that are an early hallmark of neurodegenerative diseases[60], especially in light of *SORCS1*'s link to late-onset Alzheimer's disease[61,62]. Given SorCS1's role in sorting neuronal receptors, impaired trafficking of these critical cargo proteins in the absence of SorCS1 might also contribute to the pathophysiology of the neurodevelopmental disorders with which *SORCS1* has been associated[63–66]. These observations underscore the notion that intracellular sorting is a key contributor to the proper maintenance of synaptic protein composition and function.

Acknowledgements

We thank Anders Nykjaer, Pierre Vanderhaeghen, Sara Calafate, Heather Rice, Elsa Lauwers, and Ragna Sannerud for critical reading of the manuscript and de Wit lab members for discussion and comments. We thank Casper Hoogenraad for experimental advice and reagents, and Ragna Sannerud, Catherine Faivre-Sarrailh, Rytis Prekeris, Juan S. Bonifacino, Jeremy Tavare, Lorna Hodgson, Dan P. Felsenfeld, Takeshi Sakurai, Marco Arese, Thomas C. Südhof, Peter Scheiffele, Thomas Biederer, Eunjoon Kim, Gopal Thinakaran, Ryohei Iwata, Aaron Bowen and Matthew Kennedy for reagents. We thank Lutgarde Serneels for advice on CRISPR/Cas9-based KI mouse generation, and Pieter Vanden Berghe and Valérie Van Steenbergen for live-cell imaging analysis advice and for sharing Igor-based software. L.F.R. is supported by Marie Sklodowska-Curie postdoctoral fellowship H2020-MSCA-IF-2014 and FWO Postdoctoral fellowship 12N0316N/12N0319N. B.V. is supported by FWO PhD fellowship 11A0419N. J.d.W. is supported by ERC Starting Grant (#311083); FWO Odysseus Grant; FWO Project grants G094016N and G0C4518N, FWO EOS grant G0H2818N; a Methusalem grant of KU Leuven/Flemish Government, and ERA-NET NEURON SynPathy 2015.

Author Contributions

L.F.R. and J.d.W. conceived the project and designed experiments. L.F.R. and B.V. conducted and analyzed experiments. J.N. performed characterization of *Sorcs1*^{HA} KI mice. K.M.V. assisted with molecular cloning and construct validation. K.D.W. performed electrophysiology experiments on autaptic neurons. L.F.R., B.V., J.N., K.D.W. and J.d.W. analyzed data. L.F.R. and J.d.W. wrote the paper, with input from all authors.

Declaration of Interests

The authors declare no competing interests.

References

1. Biederer, T., Kaeser, P. S. & Blanpied, T. A. Transcellular Nanoalignment of Synaptic Function. *Neuron* **96**, 680–696 (2017).

2. Emes, R. D. & Grant, S. G. N. Evolution of Synapse Complexity and Diversity. *Annu. Rev. Neurosci.* **35**, 111–131 (2012).

3. Sheng, M. & Kim, E. The Postsynaptic Organization of Synapses. *Cold Spring Harb. Perspect. Biol.* **3**, a005678–a005678 (2011).

4. Gumy, L. F. & Hoogenraad, C. C. Local mechanisms regulating selective cargo entry and long-range trafficking in axons. *Curr. Opin. Neurobiol.* **51**, 23–28 (2018).

5. Horton, A. C. & Ehlers, M. D. Neuronal polarity and trafficking. *Neuron* **40**, 277–295 (2003).

6. Bentley, M. & Banker, G. The cellular mechanisms that maintain neuronal polarity. *Nat. Rev. Neurosci.* **17**, 611–622 (2016).

7. Willnow, T. E., Petersen, C. M. & Nykjaer, A. VPS10P-domain receptors — regulators of neuronal viability and function. *Nat. Rev. Neurosci.* **9**, 899–909 (2008).

8. Hermey, G. The Vps10p-domain receptor family. *Cell. Mol. Life Sci.* **66**, 2677–2689 (2009).

9. Lane, R. F. *et al.* Protein Sorting Motifs in the Cytoplasmic Tail of SorCS1 Control Generation of Alzheimer's Amyloid- Peptide. *J. Neurosci.* **33**, 7099–7107 (2013).

10. Ma, Q. *et al.* SorCS2-mediated NR2A trafficking regulates motor deficits in Huntington's disease. *JCI Insight* **2**, (2017).

11. Subkhangulova, A. *et al.* SORCS1 and SORCS3 control energy balance and orexigenic peptide production. *EMBO Rep.* **19**, e44810 (2018).

12. Glerup, S. *et al.* SorCS2 is required for BDNF-dependent plasticity in the hippocampus. *Mol. Psychiatry* **21**, 1740–1751 (2016).

13. Savas, J. N. *et al.* The Sorting Receptor SorCS1 Regulates Trafficking of Neurexin and AMPA Receptors. *Neuron* **87**, 764–780 (2015).

14. Südhof, T. C. Synaptic Neurexin Complexes: A Molecular Code for the Logic of Neural Circuits. *Cell* **171**, 745–769 (2017).

15. Anderson, G. R. *et al.* β-Neurexins Control Neural Circuits by Regulating Synaptic Endocannabinoid Signaling. *Cell* **162**, 593–606 (2015).

16. Chen, L. Y., Jiang, M., Zhang, B., Gokce, O. & Südhof, T. C. Conditional Deletion of All Neurexins Defines Diversity of Essential Synaptic Organizer Functions for Neurexins. *Neuron* **94**, 611–625.e4 (2017).

17. Missler, M. *et al.* α-Neurexins couple Ca2+ channels to synaptic vesicle exocytosis. *Nature* **423**, 939–948 (2003).

18. Gauthier, J. *et al.* Truncating mutations in NRXN2 and NRXN1 in autism spectrum disorders and schizophrenia. *Hum. Genet.* **130**, 563–573 (2011).

19. Rees, E. *et al.* Analysis of copy number variations at 15 schizophrenia-associated loci. *Br. J. Psychiatry* **204**, 108–114 (2014).

20. Vaags, A. K. *et al.* Rare Deletions at the Neurexin 3 Locus in Autism Spectrum Disorder. *Am. J. Hum. Genet.* **90**, 133–141 (2012).

21. Ribeiro, L. F., Verpoort, B. & de Wit, J. Trafficking mechanisms of synaptogenic cell adhesion molecules. *Mol. Cell. Neurosci.* **91**, 34–47 (2018).

22. Hermey, G. *et al.* The three sorCS genes are differentially expressed and regulated by synaptic activity: sorCS genes regulated by neuronal activity. *J. Neurochem.* **88**, 1470–1476 (2004).

23. Oetjen, S., Mahlke, C., Hermans-Borgmeyer, I. & Hermey, G. Spatiotemporal expression analysis of the growth factor receptor SorCS3: Developmental expression of SorCS3. *J. Comp. Neurol.* **522**, 3386–3402 (2014).

24. Schreiner, D. *et al.* Targeted Combinatorial Alternative Splicing Generates Brain Region-Specific Repertoires of Neurexins. *Neuron* **84**, 386–398 (2014).

25. Nielsen, M. S. *et al.* Different Motifs Regulate Trafficking of SorCS1 Isoforms. *Traffic* **9**, 980–994 (2008).

26. Boncompain, G. *et al.* Synchronization of secretory protein traffic in populations of cells. *Nat. Methods* **9**, 493–498 (2012).

27. Farías, G. G., Guardia, C. M., Britt, D. J., Guo, X. & Bonifacino, J. S. Sorting of Dendritic and Axonal Vesicles at the Pre-axonal Exclusion Zone. *Cell Rep.* **13**, 1221–1232 (2015).

28. Chardin, P. & McCormick, F. Brefeldin A: the advantage of being uncompetitive. *Cell* **97**, 153–155 (1999).

29. Winckler, B. & Mellman, I. Trafficking Guidance Receptors. *Cold Spring Harb. Perspect. Biol.* **2**, a001826–a001826 (2010).

30. Barker, A. J., Koch, S. M., Reed, J., Barres, B. A. & Ullian, E. M. Developmental Control of Synaptic Receptivity. *J. Neurosci.* **28**, 8150–8160 (2008).

31. Fairless, R. *et al.* Polarized Targeting of Neurexins to Synapses Is Regulated by their C-Terminal Sequences. *J. Neurosci.* **28**, 12969–12981 (2008).

32. Taniguchi, H. *et al.* Silencing of Neuroligin Function by Postsynaptic Neurexins. *J. Neurosci.* **27**, 2815–2824 (2007).

33. Hu, Z. *et al.* Neurexin and Neuroligin Mediate Retrograde Synaptic Inhibition in C. elegans. *Science* **337**, 980–984 (2012).

34. Pregno, G. *et al.* Differential regulation of neurexin at glutamatergic and GABAergic synapses. *Front. Cell. Neurosci.* **7**, (2013).

35. Wisco, D. *et al.* Uncovering multiple axonal targeting pathways in hippocampal neurons. *J. Cell Biol.* **162**, 1317–1328 (2003).

36. Yap, C. C. *et al.* The somatodendritic endosomal regulator NEEP21 facilitates axonal targeting of L1/NgCAM. *J. Cell Biol.* **180**, 827–842 (2008).

37. Bel, C., Oguievetskaia, K., Pitaval, C., Goutebroze, L. & Faivre-Sarrailh, C. Axonal targeting of Caspr2 in hippocampal neurons via selective somatodendritic endocytosis. *J. Cell Sci.* **122**, 3403–3413 (2009).

38. Horgan, C. P. & McCaffrey, M. W. The dynamic Rab11-FIPs. *Biochem. Soc. Trans.* **37**, 1032–1036 (2009).

39. Prekeris, R., Klumperman, J. & Scheller, R. H. A Rab11/Rip11 protein complex regulates apical membrane trafficking via recycling endosomes. *Mol. Cell* **6**, 1437–1448 (2000).

40. Su, T. *et al.* A kinase cascade leading to Rab11-FIP5 controls transcytosis of the polymeric immunoglobulin receptor. *Nat. Cell Biol.* **12**, 1143–1153 (2010).

41. Meyers, J. M. & Prekeris, R. Formation of Mutually Exclusive Rab11 Complexes with Members of the Family of Rab11-interacting Proteins Regulates Rab11 Endocytic Targeting and Function. *J. Biol. Chem.* **277**, 49003–49010 (2002).

42. Gokce, O. & Sudhof, T. C. Membrane-Tethered Monomeric Neurexin LNS-Domain Triggers Synapse Formation. *J. Neurosci.* **33**, 14617–14628 (2013).

43. Scheiffele, P., Fan, J., Choih, J., Fetter, R. & Serafini, T. Neuroligin expressed in nonneuronal cells triggers presynaptic development in contacting axons. *Cell* **101**, 657–669 (2000).

44. Woo, J. *et al.* Trans-synaptic adhesion between NGL-3 and LAR regulates the formation of excitatory synapses. *Nat. Neurosci.* **12**, 428–437 (2009).

45. Zhang, C. *et al.* Neurexins Physically and Functionally Interact with GABAA Receptors. *Neuron* **66**, 403–416 (2010).

46. Turrigiano, G. G., Leslie, K. R., Desai, N. S., Rutherford, L. C. & Nelson, S. B. Activity-dependent scaling of quantal amplitude in neocortical neurons. *Nature* **391**, 892–896 (1998).

47. Schonteich, E. *et al.* The Rip11/Rab11-FIP5 and kinesin II complex regulates endocytic protein recycling. *J. Cell Sci.* **121**, 3824–3833 (2008).

48. Garcia-Castillo, M. D., Chinnapen, D. J.-F. & Lencer, W. I. Membrane Transport across Polarized Epithelia. *Cold Spring Harb. Perspect. Biol.* **9**, a027912 (2017).

49. Craig, A. M. & Banker, G. Neuronal Polarity. *Annu. Rev. Neurosci.* **17**, 267–310 (1994).

50. Ascano, M., Richmond, A., Borden, P. & Kuruvilla, R. Axonal Targeting of Trk Receptors via Transcytosis Regulates Sensitivity to Neurotrophin Responses. *J. Neurosci.* **29**, 11674–11685 (2009).

51. Leterrier, C. Constitutive Activation Drives Compartment-Selective Endocytosis and Axonal Targeting of Type 1 Cannabinoid Receptors. *J. Neurosci.* **26**, 3141–3153 (2006).

52. Buggia-Prévot, V. *et al.* A Function for EHD Family Proteins in Unidirectional Retrograde Dendritic Transport of BACE1 and Alzheimer's Disease Aβ Production. *Cell Rep.* **5**, 1552–1563 (2013).

53. Li, P., Merrill, S. A., Jorgensen, E. M. & Shen, K. Two Clathrin Adaptor Protein Complexes Instruct Axon-Dendrite Polarity. *Neuron* **90**, 564–580 (2016).

54. Lin, D.-T. *et al.* Regulation of AMPA receptor extrasynaptic insertion by 4.1N, phosphorylation and palmitoylation. *Nat. Neurosci.* **12**, 879–887 (2009).

55. Yamashita, N., Joshi, R., Zhang, S., Zhang, Z.-Y. & Kuruvilla, R. Phospho-Regulation of Soma-to-Axon Transcytosis of Neurotrophin Receptors. *Dev. Cell* **42**, 626–639.e5 (2017).

56. Chanda, S., Hale, W. D., Zhang, B., Wernig, M. & Südhof, T. C. Unique versus Redundant Functions of Neuroligin Genes in Shaping Excitatory and Inhibitory Synapse Properties. *J. Neurosci.* **37**, 6816–6836 (2017).

57. Schroeder, A. *et al.* A Modular Organization of LRR Protein-Mediated Synaptic Adhesion Defines Synapse Identity. *Neuron* **99**, 329–344.e7 (2018).

58. Kattenstroth, G., Tantalaki, E., Sudhof, T. C., Gottmann, K. & Missler, M. Postsynaptic N-methyl-D-aspartate receptor function requires -neurexins. *Proc. Natl. Acad. Sci.* **101**, 2607–2612 (2004).

59. Tong, X.-J. *et al.* Retrograde Synaptic Inhibition Is Mediated by α-Neurexin Binding to the α2δ Subunits of N-Type Calcium Channels. *Neuron* **95**, 326–340.e5 (2017).

60. Cataldo, A. *et al.* Endocytic disturbances distinguish among subtypes of Alzheimer's disease and related disorders. *Ann. Neurol.* **50**, 661–665 (2001).

61. Grupe, A. *et al.* A Scan of Chromosome 10 Identifies a Novel Locus Showing Strong Association with Late-Onset Alzheimer Disease. *Am. J. Hum. Genet.* **78**, 78–88 (2006).

62. Reitz, C. *et al.* SORCS1 alters amyloid precursor protein processing and variants may increase Alzheimer's disease risk. *Ann. Neurol.* **69**, 47–64 (2011).

63. Christoforou, A. *et al.* Convergence of linkage, association and GWAS findings for a candidate region for bipolar disorder and schizophrenia on chromosome 4p. *Mol. Psychiatry* **16**, 240–242 (2011).

64. Lionel, A. C. *et al.* Rare Copy Number Variation Discovery and Cross-Disorder Comparisons Identify Risk Genes for ADHD. *Sci. Transl. Med.* **3**, 95ra75-95ra75 (2011).

65. Ollila, H. M. *et al.* Findings from bipolar disorder genome-wide association studies replicate in a Finnish bipolar family-cohort. *Mol. Psychiatry* **14**, 351–353 (2009).

66. Sanders, S. J. *et al.* De novo mutations revealed by whole-exome sequencing are strongly associated with autism. *Nature* **485**, 237–241 (2012).

FIGURES and FIGURE LEGENDS

Figure 1

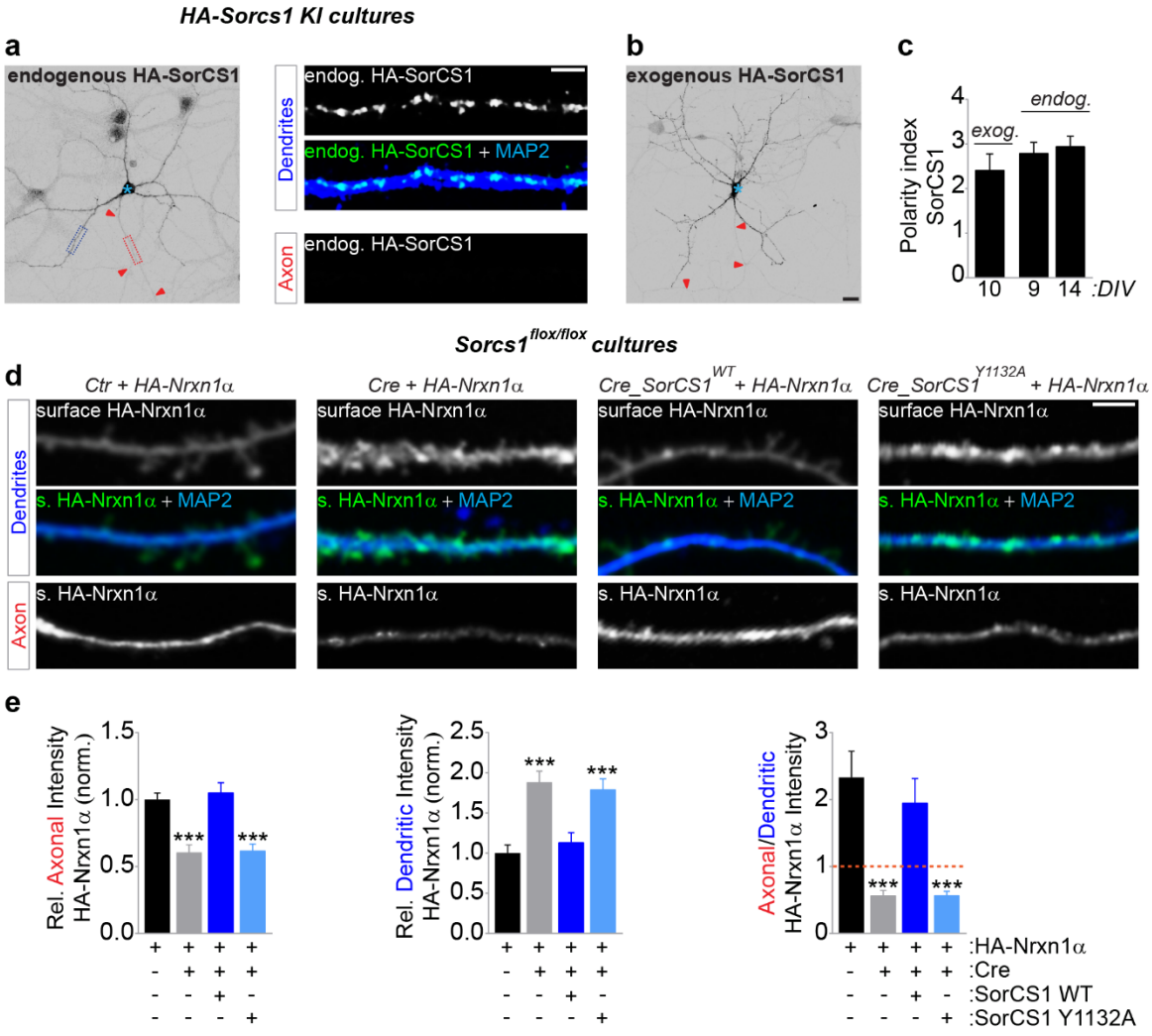

Figure 1. Axonal Polarization of Neurexin1α Requires SorCS1-Mediated Sorting in Dendrites

(a) DIV9 *Sorcs1*$^{HA/HA}$ mouse cortical neurons immunostained for HA-SorCS1 (grayscale and green), MAP2 (blue) and Ankyrin-G (not shown). Red arrowheads indicate the axon and blue asterisk marks the cell body. High-zoom images show dendritic (dotted blue box) and axonal (dotted red box) distribution of endogenous SorCS1.

(b) DIV10 WT mouse hippocampal neurons expressing HA-SorCS1 immunostained for HA-SorCS1 in grayscale; MAP2 and Ankyrin-G (not shown).

(c) Quantification of (a and b): dendritic versus axonal distribution (D:A – polarity index) of endogenous (DIV9, n = 26 neurons and DIV14, n = 26) and exogenous (n = 14) SorCS1 from 3 and 2 independent experiments, respectively.

(d) DIV8–DIV10 *Sorcs1*$^{flox/flox}$ mouse cortical neurons electroporated with EGFP (Ctr), Cre-EGFP, Cre-EGFP-T2A-SorCS1^{WT} or Cre-EGFP-T2A-SorCS1^{Y1132A} and transfected with HA-Nrxn1α, immunostained for surface HA-Nrxn1α (grayscale and green), MAP2 (blue); Ankyrin-G and GFP (not shown).

(e) Quantification of (d): surface HA-Nrxn1α fluorescence intensity in axon and dendrites relative to total surface levels and normalized to cells expressing EGFP and ratio of axonal/dendritic surface HA intensity. Ctr (n = 28 neurons); Cre (n = 29); Cre_SorCS1^{WT} (n = 28); Cre_SorCS1^{Y1132A} (n = 28). ***p < 0.001 (Kruskal-Wallis test followed by Dunn's multiple comparisons test, 3 independent experiments).

Graphs show mean ± SEM. Scale bars, 20 µm (whole cell panels); 5 µm (high-zoom images).

Figure 2

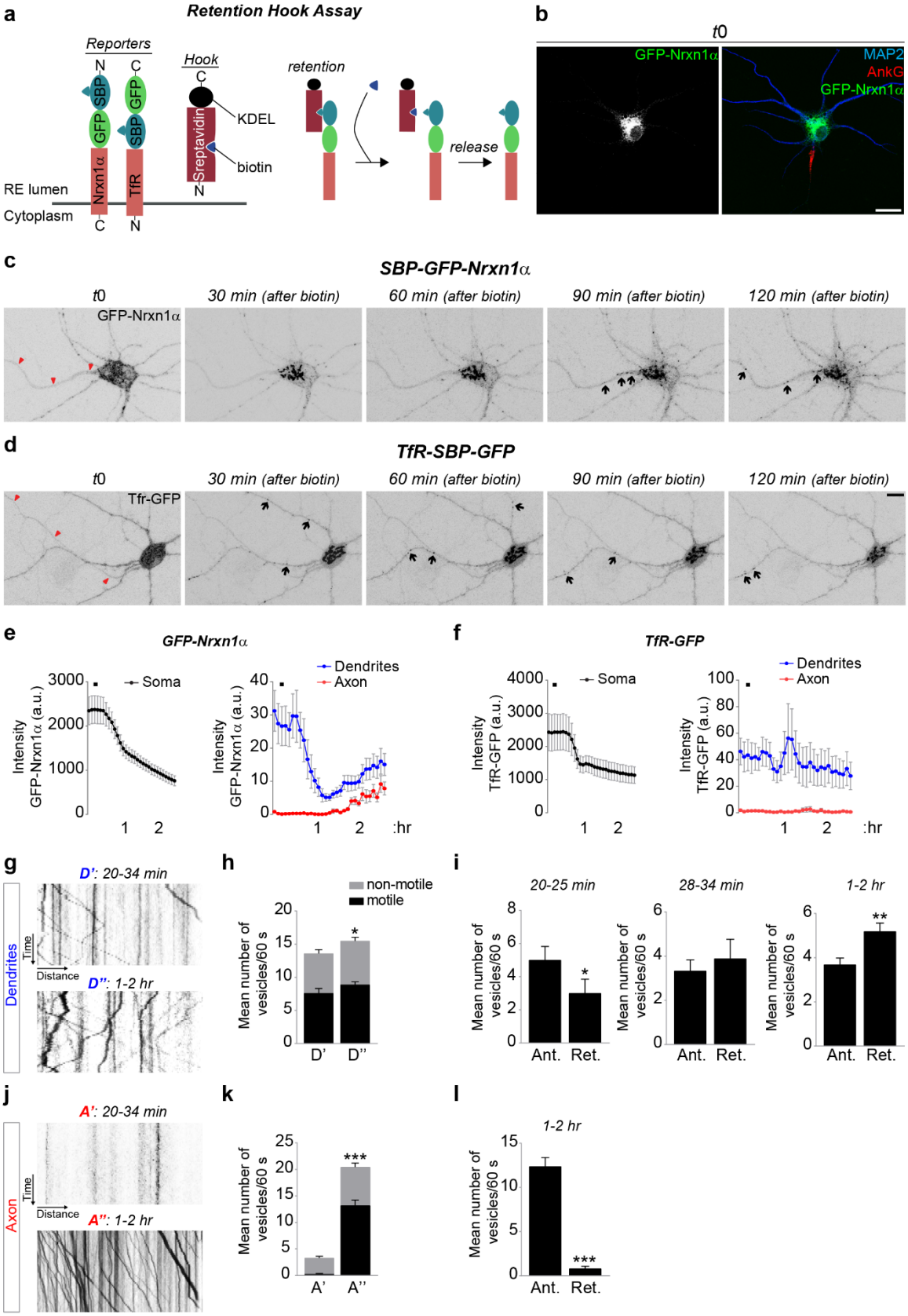

Figure 2. Delayed Axonal Trafficking of Neurexin1α

(a) Schematic representation of streptavidin-KDEL (ER hook) and reporters (Nrxn1α and TfR) used in the RUSH experiments. Addition of biotin dissociates the reporters from the ER hook, inducing synchronous release from the ER and transport through the secretory pathway.

(b) DIV9 WT mouse cortical neuron co-expressing SBP-GFP-Nrxn1α and streptavidin-KDEL immunostained for MAP2 (blue), Ankyrin-G (red) and GFP-Nrxn1α (grayscale and green).

(c–f) Live-cell imaging in DIV8–DIV10 WT rat cortical neurons co-expressing SBP-GFP-Nrxn1α and ER hook or TfR-SBP-GFP and ER hook. After 24–31 hr of expression neurons were imaged every 5 min for 2.5 hr. Biotin was added 10 min after the beginning of the imaging session. See also **Supplementary Movies 1** e **2**.

(c and d) Representative images of GFP-Nrxn1α (c) and TfR-GFP (d) fluorescence in dendrites and axon before (*t*0) and 30, 60, 90 and 120 min after adding biotin. Red arrowheads indicate axon and black arrows indicate GFP-Nrxn1α- or TfR-GFP-positive puncta.

(e and f) Quantification of GFP-Nrxn1α (n = 23 neurons) and TfR-GFP (n = 13) fluorescence intensity in soma, dendrites and axon in 3 independent experiments.

(g–l) Live-cell imaging in DIV8–DIV10 WT rat cortical neurons co-expressing SBP-GFP-Nrxn1α and ER hook. After 21–30 hr of expression neurons were imaged every second for 60–120s either 20–34 min or 1–2 hr after adding biotin. See also **Supplementary Movies 5** e **6**.

(g and j) Kymographs illustrating GFP-Nrxn1α vesicle dynamics over a 60s period in dendrites [D] and axons [A] from neurons treated with biotin for either 25 min or 2 hr.

(h and k) Mean number of motile and non-motile GFP-Nrxn1α vesicles in dendrites [D] and axons [A] from neurons treated with biotin for either 20–34 min (n = 17 neurons) or 1–2 hr (n = 16) in 2 and 3 independent experiments, respectively.

(i and l) Mean number of GFP-Nrxn1α vesicles moving in anterograde and retrograde direction in dendrites and axons. In dendrites analysis was performed at 3 different time intervals: 20–25 min (n = 8 neurons), 28–34 min (n = 9) and 1–2 hr after adding biotin; in axons analysis was performed 1–2 hr after biotin.

Graphs show mean ± SEM. *p < 0.05; **p < 0.01; ***p < 0.001 (Mann-Whitney test). Scale bars, 20 μm (b); 10 μm (d).

Figure 3

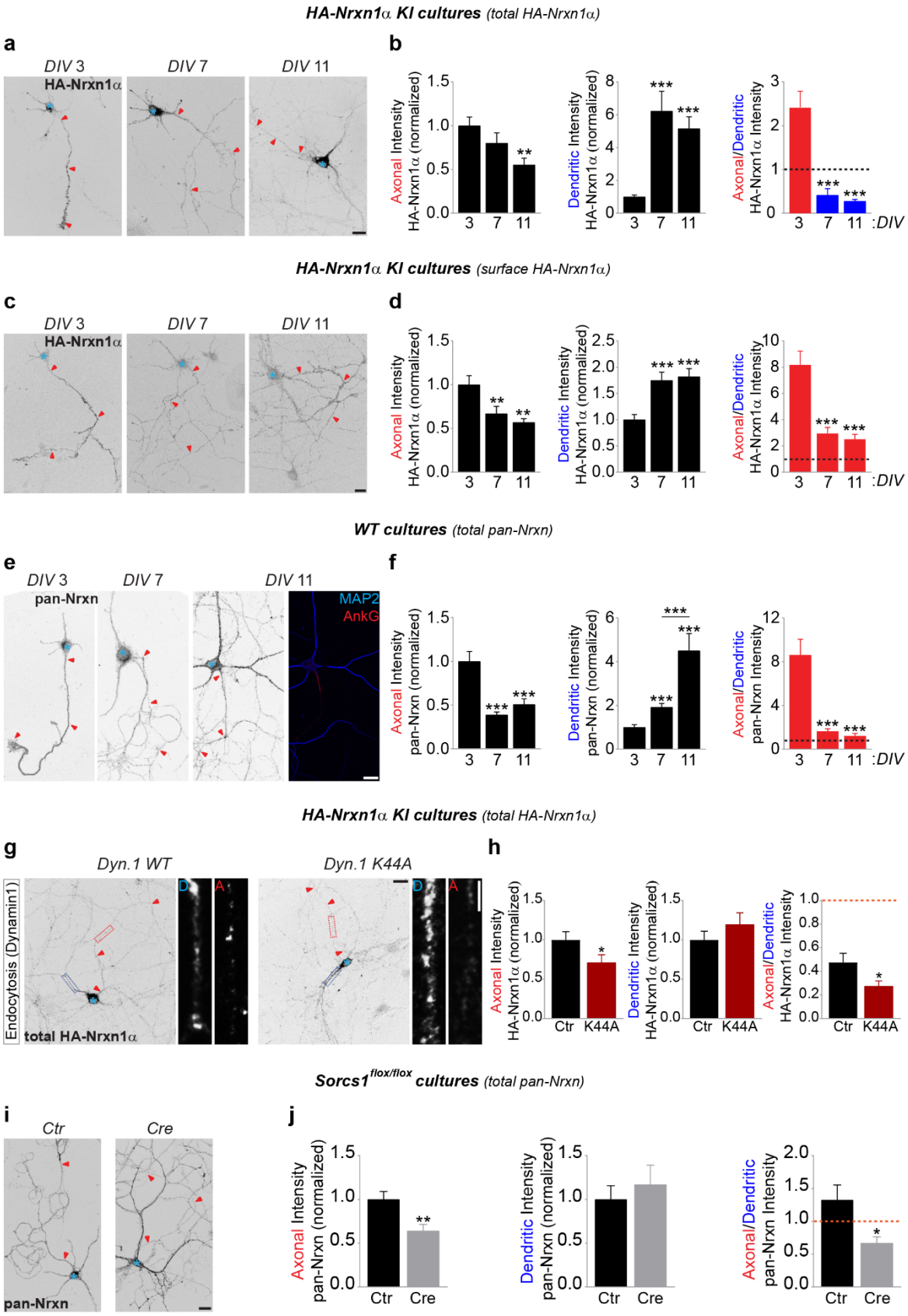

Figure 3. Endogenous Neurexins Localize to the Somatodendritic Compartment and Axonal Compartment in an Endocytosis- and SorCS1-Dependent Manner

(a) Permeabilized DIV3, DIV7 and DIV11 *Nrxn1α*$^{HA/HA}$ mouse cortical neurons labeled with an HA antibody (grayscale images inverted for clarity). Red arrowheads indicate the axon and blue asterisk marks the cell body.

(b) Quantification of (a): HA-Nrxn1α fluorescence intensity in axon and dendrites normalized to DIV3 neurons and ratio of axonal/dendritic HA intensity. DIV3 (n = 38 neurons); DIV7 (n = 30); DIV11 (n = 30). **p < 0.01; ***p < 0.001 (Kruskal-Wallis test followed by Dunn's multiple comparisons test, at least 3 independent cultures).

(c) Non-permeabilized DIV3, DIV7 and DIV11 *Nrxn1α*$^{HA/HA}$ cortical neurons surface labeled with an HA antibody.

(d) Quantification of (c): surface HA-Nrxn1α fluorescence intensity in axon and dendrites normalized to DIV3 neurons and ratio of axonal/dendritic surface HA intensity. DIV3 (n = 30 neurons); DIV7 (n = 29); DIV11 (n = 24). **p < 0.01; ***p < 0.001 (Kruskal-Wallis test followed by Dunn's multiple comparisons test, 3 independent cultures).

(e) Permeabilized DIV3, DIV7 and DIV11 WT mouse cortical neurons labeled with a pan-Nrxn antibody (grayscale). MAP2 (blue) and Ankyrin-G (AnkG; red) identify somatodendritic and axonal compartments, respectively.

(f) Quantification of (e): pan-Nrxn fluorescence intensity in axon and dendrites normalized to DIV3 neurons and ratio of axonal/dendritic pan-Nrxn intensity. DIV3 (n = 30 neurons); DIV7 (n = 30); DIV11 (n = 29). ***p < 0.001 (Kruskal-Wallis test followed by Dunn's multiple comparisons test, 3 independent cultures).

(g) DIV8, DIV10 *Nrxn1α*$^{HA/HA}$ mouse cortical neurons expressing WT (Ctr) or K44A Dyn.1 labeled for total HA-Nrxn1α. High-zoom images of dendritic [D, dotted blue box] and axonal [A, dotted red box] Nrxn1α are shown next to the whole cell images.

(h) Quantification of (g): HA-Nrxn1α fluorescence intensity in axon and dendrites normalized to cells expressing Dyn.1 WT and ratio of axonal/dendritic HA intensity. Ctr (n = 30 neurons); K44A (n = 29). *p < 0.05 (Mann-Whitney test, 3 independent cultures).

(i) DIV10 *Sorcs1*$^{flox/flox}$ cortical neurons electroporated with EGFP (Ctr) or Cre-EGFP immunostained for pan-Nrxn in grayscale; MAP2, Ankyrin-G and GFP (not shown).

(j) Quantification of (i): pan-Nrxn fluorescence intensity in axon and dendrites normalized to cells expressing EGFP and ratio of axonal/dendritic pan-Nrxn intensity. Ctr (n = 30 neurons); Cre (n = 29). *p < 0.05; **p < 0.01 (Mann-Whitney test, 3 independent cultures).

Graphs show mean ± SEM. Scale bars, 20 µm (whole cell panels); 5 µm (high-zoom images).

Figure 4.

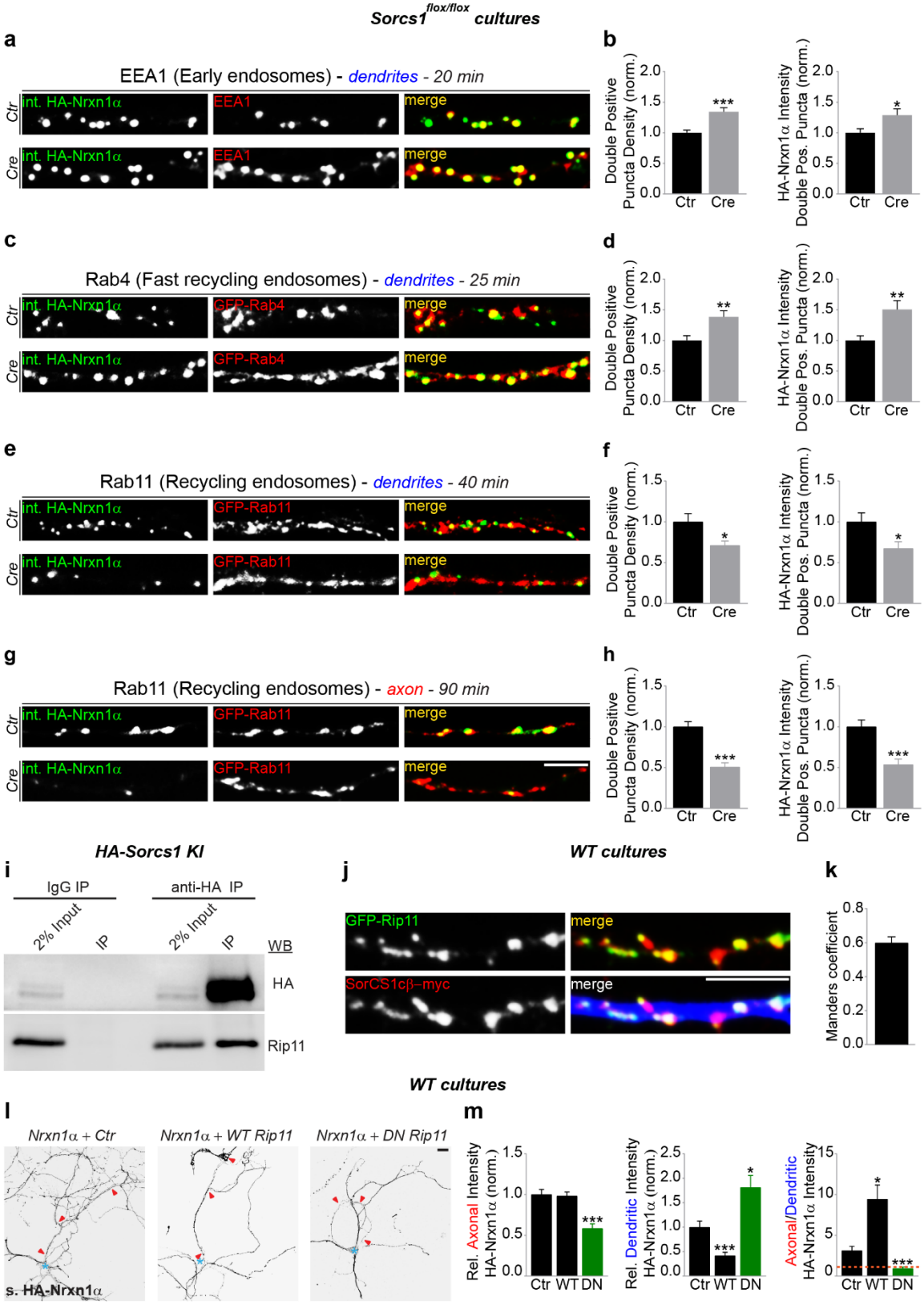

Figure 4. SorCS1 Interacts with Rip11 to Control Neurexin1α Transition from Early to Recycling Endosomes

(a) DIV8–DIV10 *Sorcs1*$^{flox/flox}$ cortical neurons electroporated with mCherry (Ctr) or Cre-T2A-mCherry and transfected with HA-Nrxn1α (pulse-chased for 20 min), labeled for internalized HA-Nrxn1α (grayscale), EEA1 (red) and Ankyrin-G (not shown).

(b) Quantification of (a): number of internalized Nrxn1α- and EEA1-double positive puncta normalized to cells expressing mCherry, and intensity of internalized Nrxn1α fluorescence in the double-positive puncta normalized to cells expressing mCherry. Ctr (n = 26 neurons); Cre (n = 25). *p < 0.05; ***p < 0.001 (Mann-Whitney test, 3 independent experiments).

(c) DIV8–DIV10 *Sorcs1*$^{flox/flox}$ cortical neurons electroporated with mCherry (Ctr) or Cre-T2A-mCherry and co-transfected with HA-Nrxn1α and GFP-Rab4 (pulse-chased for 25 min), labeled for internalized HA-Nrxn1α (grayscale), GFP-Rab4 (red) and Ankyrin-G (not shown).

(d) Quantification of (c); Ctr (n = 28 neurons); Cre (n = 26). **p < 0.01 (Mann-Whitney test, 3 independent experiments).

(e) DIV8–DIV10 *Sorcs1*$^{flox/flox}$ cortical neurons electroporated with mCherry (Ctr) or Cre-T2A-mCherry and co-transfected with HA-Nrxn1α and GFP-Rab11 (pulse-chased for 40 min), labeled for internalized HA-Nrxn1α (grayscale), GFP-Rab11 (red) and Ankyrin-G (not shown).

(f) Quantification of (e); Ctr (n = 29 neurons); Cre (n = 23). *p < 0.05 (Mann-Whitney test, 3 independent experiments).

(g) DIV8–DIV10 *Sorcs1*$^{flox/flox}$ cortical neurons electroporated with mCherry (Ctr) or Cre-T2A-mCherry and co-transfected with HA-Nrxn1α and GFP-Rab11 (pulse-chased for 90 min), labeled for internalized HA-Nrxn1α (grayscale), GFP-Rab11 (red) and Ankyrin-G (not shown).

(h) Quantification of (g); Ctr (n = 28 neurons); Cre (n = 26). ***p < 0.001 (Mann-Whitney test, 3 independent experiments).

(i) Western blot for the recovery of Rip11 in immunoprecipitated HA-SorCS1 complexes from P21–P28 mouse *Sorcs1*$^{HA/HA}$ KI-cortical prey extracts.

(j) DIV9–DIV10 WT cortical neurons co-expressing EGFP-Rip11 and SorCS1cβ-myc immunostained for GFP-Rip11 (grayscale and green), SorCS1-myc (grayscale and red) and MAP2 (blue).

(k) Quantification of the colocalization of Rip11 with SorCS1 expressed as Manders coefficient (n = 20) in 2 independent experiments.

(l) DIV9 WT cortical neurons co-expressing HA-Nrxn1α and EGFP (Ctr), WT EGFP-Rip11 or dominant-negative (DN) EGFP-Rip11, and immunostained for surface HA-Nrxn1α (grayscale); MAP2, Ankyrin-G and GFP (not shown). Red arrowheads indicate the axon and blue asterisk marks the cell body.

(m) Quantification of (l): surface HA-Nrxn1α fluorescence intensity in axon and dendrites relative to total surface levels and normalized to cells expressing EGFP and ratio of axonal/dendritic surface HA intensity (n = 30 for each group). *p < 0.05; ***p < 0.001 (Kruskal-Wallis test followed by Dunn's multiple comparisons test, 3 independent experiments).

Graphs show mean ± SEM. Scale bars, 5 µm (g and j); 20 µm (l).

Figure 5.

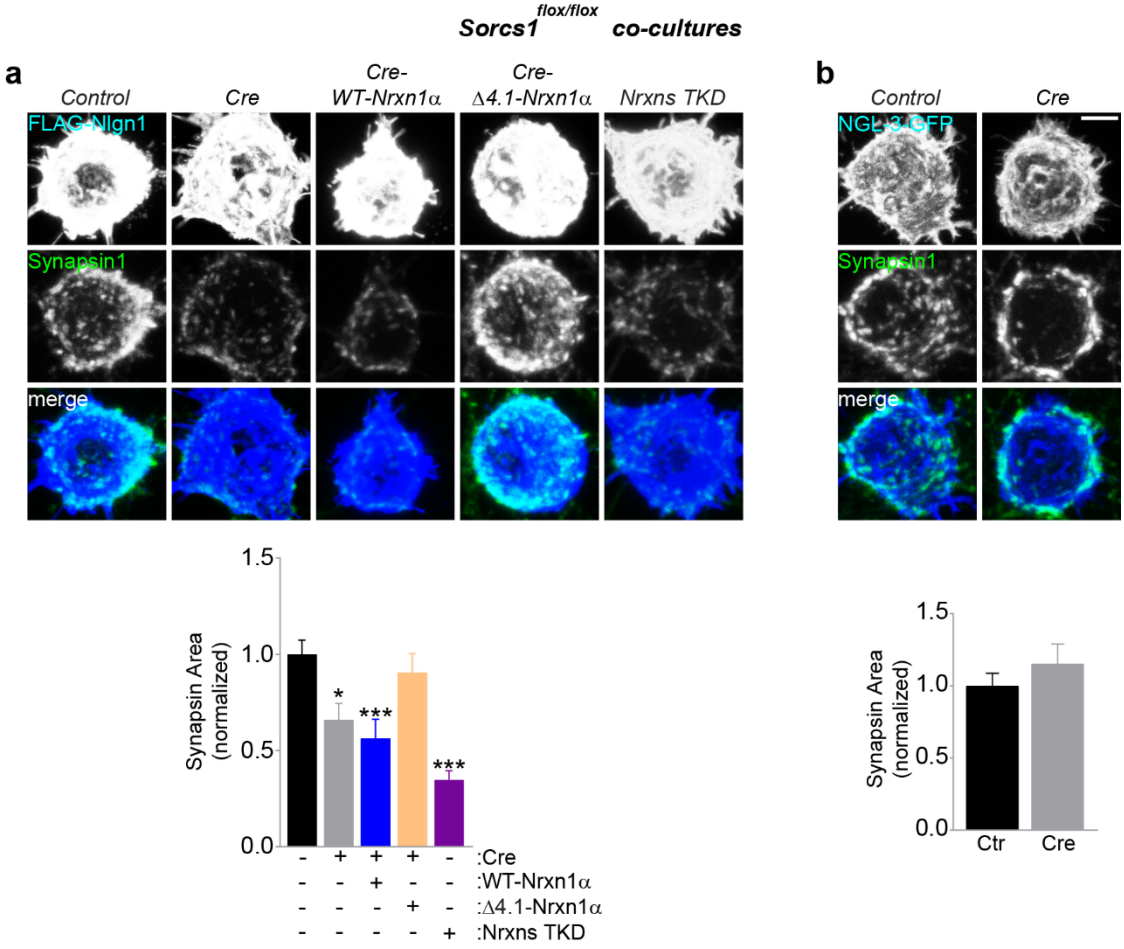

Figure 5. Loss of SorCS1 Impairs Neurexin-Mediated Synaptogenesis

(a and b, upper) HEK293T-cells expressing FLAG-Nlgn1 or NGL-3-GFP co-cultured with DIV10 *Sorcs1*$^{flox/flox}$ cortical neurons, previously infected with lentivirus expressing mCherry (Control), Cre-T2A-mCherry, Cre-T2A-mCherry-T2A-Nrxn1α-WT, Cre-T2A-mCherry-T2A-Nrxn1αΔ4.1 or Nrxn TKD; immunostained for FLAG-Nlgn1 or NGL-3-GFP (blue), Synapsin1 (green) and mCherry (not shown). Scale bar, 5 μm.

(a and b, lower) Quantification of the area of Synapsin1 clustering on the surface of Nlgn1- or NGL-3-expressing HEK cells and normalized to cells expressing mCherry. Nlgn1: Control (n = 29 neurons); Cre (n = 30); Cre-WT (n = 30); Cre-Δ4.1 (n = 30); TKD Nrxns (n = 30). NGL-3: Control (n = 30); Cre (n = 30). *p < 0.05; ***p < 0.001 (Kruskal-Wallis test followed by Dunn's multiple comparisons test, 3 independent experiments). Graphs show mean ± SEM.

Figure 6.

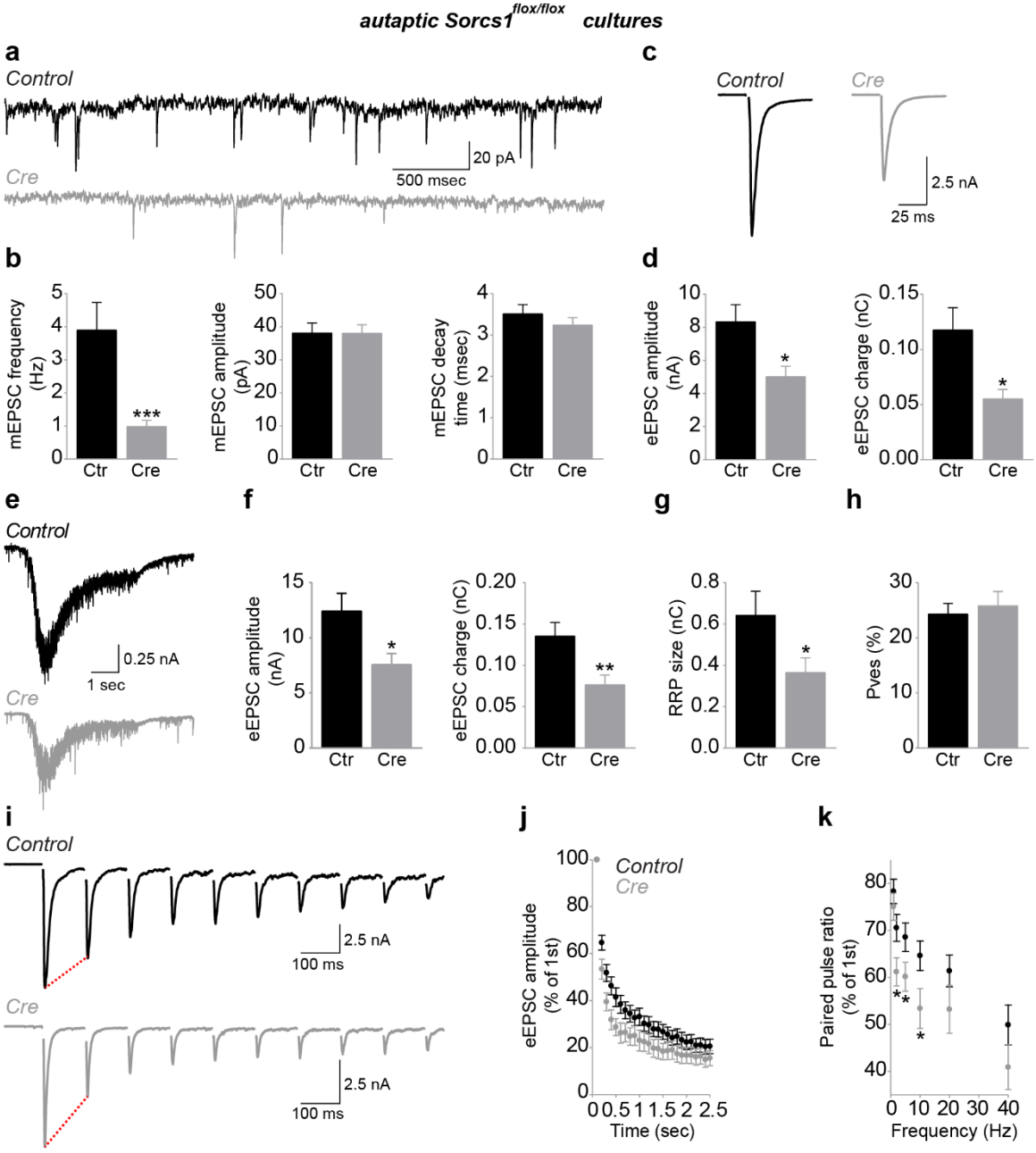

Figure 6. Loss of SorCS1 Impairs Presynaptic Function

(a) Example traces of mEPSCs recorded from DIV14–DIV16 *Sorcs1*$^{flox/flox}$ autaptic cortical neurons electroporated with EGFP (Control) or Cre-EGFP.

(b) mEPSC frequency, but not amplitude and decay time, is decreased in *Sorcs1* KO neurons. Control (n = 18 neurons); Cre (n = 15). ***p < 0.001 (Mann-Whitney test, 3 independent experiments).

(c) Example traces of eEPSC recorded from DIV14–DIV16 *Sorcs1*$^{flox/flox}$ autaptic cortical neurons electroporated with EGFP (Control) or Cre-EGFP.

(d) eEPSC amplitude and eEPSC charge are decreased in *Sorcs1* KO neurons. Control (n = 17 neurons); Cre (n = 13). *p < 0.05 (Mann-Whitney test, 4 independent experiments).

(e) Example traces of sucrose responses recorded from DIV14 *Sorcs1*$^{flox/flox}$ autaptic cortical neurons electroporated with EGFP (Control) or Cre-EGFP.

(f–h) Decreased eEPSC amplitude, eEPSC charge (f) and readily releasable pool (RRP) size (g) in *Sorcs1* KO neurons, but vesicular release probability (Pves) is unaffected (h). Control (n = 17 neurons); Cre (n = 21). *p < 0.05; **p < 0.01 (Mann-Whitney test, 3 independent experiments).

(i) Example traces of train stimulations (10 Hz) recorded from DIV14–DIV16 *Sorcs1*$^{flox/flox}$ autaptic cortical neurons electroporated with EGFP (Control) or Cre.

(j) Increased depression during 10 Hz stimulation in *Sorcs1* KO neurons. Control (n = 18 neurons); Cre (n = 14); 3 independent experiments.

(k) Increased paired-pulse depression in *Sorcs1* KO neurons throughout different inter-stimulation intervals. Control (n = 14 neurons); Cre (n = 18). *p < 0.05 (two-tailed t-test, 3 independent experiments). Graphs show mean ± SEM.

Figure 7.

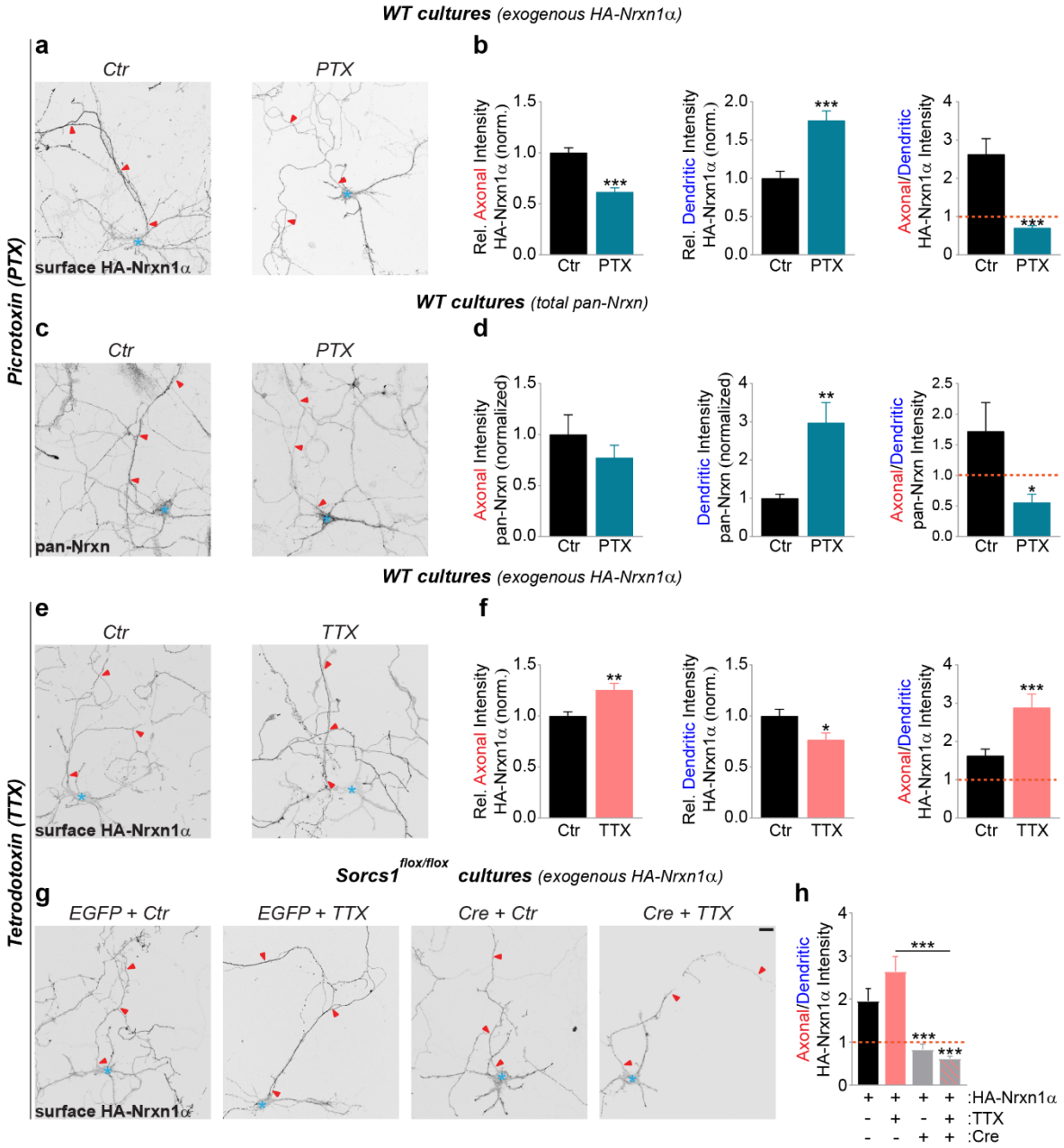

Figure 7. Activity Controls Bidirectionally the Axonal/Dendritic Surface Balance of Neurexin1α

(a) DIV8–DIV10 WT mouse cortical neurons expressing HA-Nrxn1α and treated with DMSO (Ctr) or picrotoxin (PTX) for 48 hr, immunostained for surface HA-Nrxn1α (grayscale); MAP2 and Ankyrin-G (not shown). Red arrowheads indicate the axon and blue asterisk marks the cell body.

(b) Quantification of (a): surface HA-Nrxn1α fluorescence intensity in axon and dendrites relative to total surface levels and normalized to cells treatead with DMSO and ratio of axonal/dendritic surface HA intensity. Ctr (n = 30 neurons); PTX (n = 30). ***p < 0.001 (Mann-Whitney test, 3 independent experiments).

(c) DIV8–DIV10 WT mouse cortical neurons treated with DMSO (Ctr) or picrotoxin (PTX) for 48 hr, immunostained for pan-Nrxn (grayscale); MAP2 and Ankyrin-G (not shown).

(d) Quantification of (c): pan-Nrxn fluorescence intensity in axon and dendrites normalized to cells treatead with DMSO and ratio of axonal/dendritic pan-Nrxn intensity. Ctr (n = 26 neurons); PTX (n = 28). *p < 0.05; **p < 0.01 (Mann-Whitney test, 3 independent cultures).

(e) DIV8–DIV10 WT mouse cortical neurons expressing HA-Nrxn1α untreated (Ctr) or treated with tetrodotoxin (TTX) for 48 hr, immunostained for surface HA-Nrxn1α (grayscale); MAP2 and Ankyrin-G (not shown).

(f) Quantification of (e): surface HA-Nrxn1α fluorescence intensity in axon and dendrites relative to total surface levels and normalized to control cells and ratio of axonal/dendritic surface HA intensity. Ctr (n = 30 neurons); TTX (n = 29). ***p < 0.001 (Mann-Whitney test, 3 independent experiments).

(g) DIV8–DIV10 *Sorcs1*$^{flox/flox}$ mouse cortical neurons electroporated with EGFP or Cre-EGFP and transfected with HA-Nrxn1α untreated (Ctr) or treated with tetrodotoxin (TTX) for 48 hr, immunostained for surface HA-Nrxn1α (grayscale); MAP2, Ankyrin-G and GFP (not shown).

(h) Quantification of (g): surface HA-Nrxn1α fluorescence intensity in axon and dendrites relative to total surface levels and normalized to cells expressing EGFP untreated and ratio of axonal/dendritic surface HA intensity. EGFP_Ctr (n = 35 neurons); EGFP_TTX (n = 35); Cre_Ctr (n = 36); Cre_TTX (n = 35). ***p < 0.001 (Kruskal-Wallis test followed by Dunn's multiple comparisons test, 4 independent experiments). Graphs show mean ± SEM. Scale bar, 20 μm.

Supplementary Information

SorCS1-mediated Sorting of Neurexin in Dendrites Maintains Presynaptic Function

Luís F. Ribeiro[1,2], Ben Verpoort[1,2], Julie Nys[1,2], Kristel M. Vennekens[1,2], Keimpe D. Wierda[1,2] and Joris de Wit[1,2,*]

Affiliations:
[1]VIB Center for Brain & Disease Research, Herestraat 49, B-3000 Leuven, Belgium
[2]KU Leuven, Department of Neurosciences, Leuven Brain Institute, Herestraat 49, B-3000 Leuven, Belgium

[*]**Correspondence**: joris.dewit@kuleuven.vib.be

SUPPLEMENTARY FIGURES and FIGURE LEGENDS

Supplementary Figure 1.

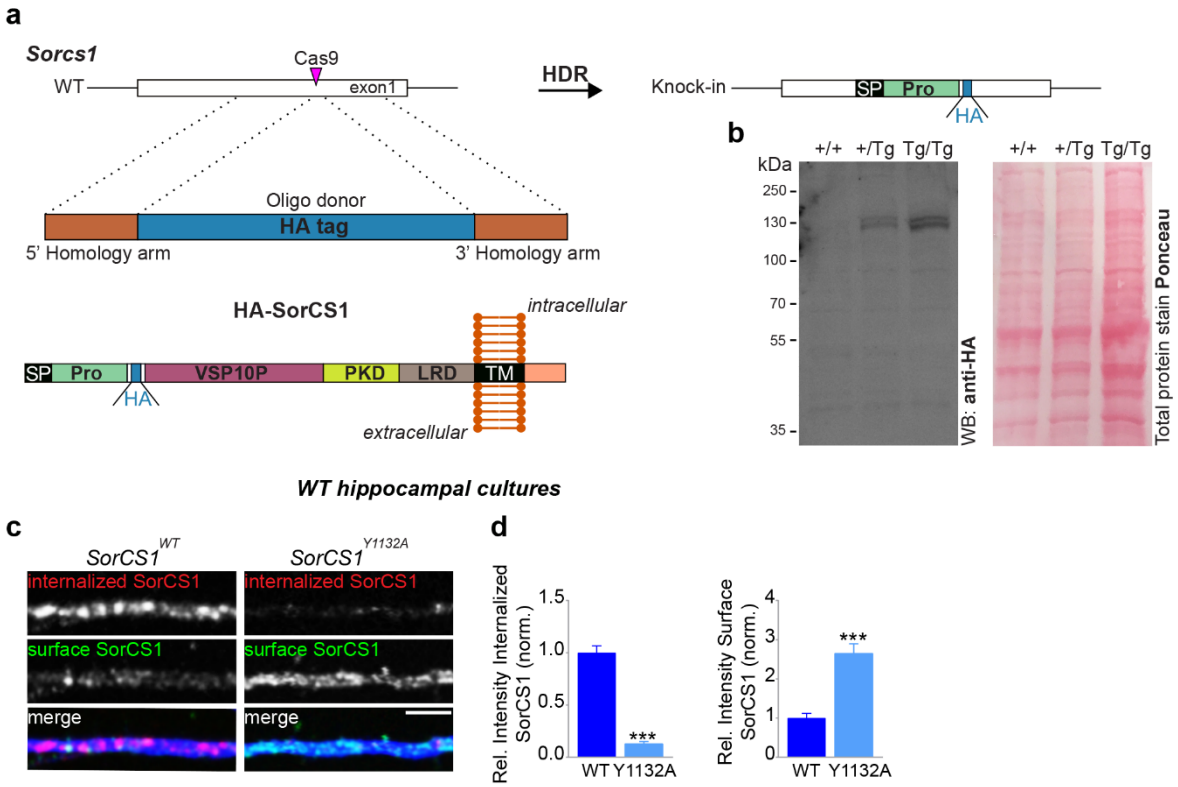

Supplementary Figure 1. *Sorcs1*$^{HA/HA}$ KI mouse generation and validation of SorCS1 endocytosis-defective mutant (Y1132A).

(a and b) *Sorcs1*$^{HA/HA}$ KI mouse generation and validation.

(a) Orange boxes represent the left and right homologous arms. Blue box represents the single-strand DNA (ssDNA) donor oligonucleotide containing the HA-tag. CRISPR/Cas9-mediated homology directed repair (HDR) allowed for precise HA-tagging of the *Sorcs1* locus. Schematic representation of SorCS1 protein domain organization is shown to illustrate the HA-tagging of HA-SorCS1 downstream of the second furin cleavage site, right before the VPS10P domain (at the amino acid position 144). Domain abbreviations: SP, signal peptide; Pro, pro-peptide; VPS10P, vacuolar protein sorting 10 protein; PKD, polycystic kidney disease domain; LRD, leucine-rich domain; TM, transmembrane.

(b) Detection of HA-SorCS1 by western blot in total brain extracts prepared from *Sorcs1*$^{HA/HA}$ KI mice (P60). Total protein staining by using Ponceau method was used as loading control.

(c and d) Validation of SorCS1 endocytosis-defective mutant (Y1132A).

(c) High-zoom images of dendritic internalized and surface SorCS1 from DIV9 WT mouse hippocampal neurons expressing extracellular HA-tagged WT SorCS1cβ (WT) or Y1132A for 48 hr. Live neurons were incubated with an anti-HA antibody and pulse-chased for 20 min. Neurons were immunostained for surface HA-SorCS1 (grayscale and green), internalized SorCS1 (grayscale and red) and MAP2 (blue). Scale bar, 5 μm.

(d) Quantification of (c): internalized SorCS1 fluorescence intensity relative to total levels and normalized to cells expressing WT-SorCS1; surface SorCS1 fluorescence intensity relative to total levels and normalized to cells expressing WT-SorCS1. WT (n = 28 neurons); Y1132A (n = 30). ***p < 0.001 (Mann-Whitney test, 3 independent experiments). Graphs show mean ± SEM.

Supplementary Figure 2.

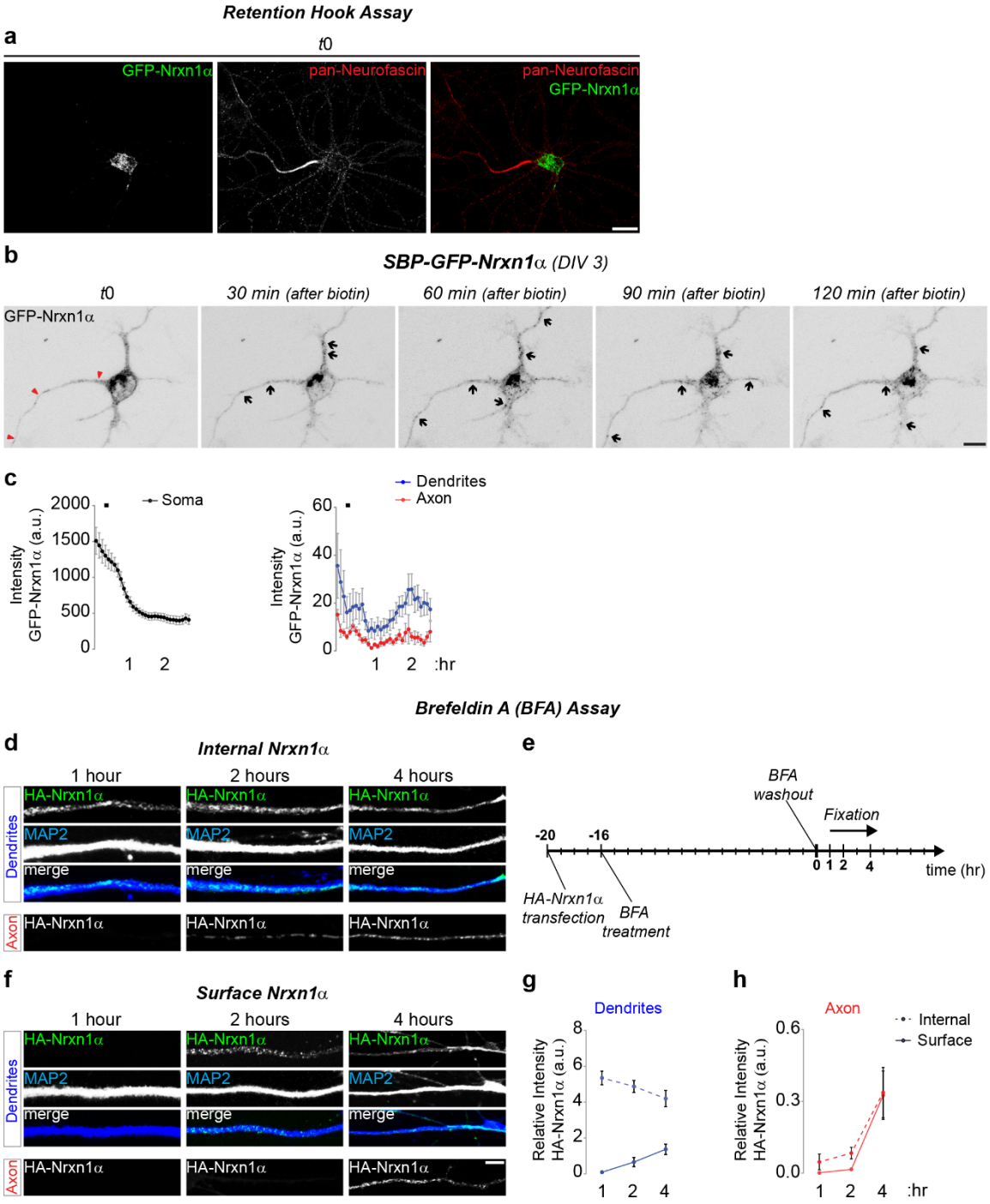

Supplementary Figure 2. Delayed axonal trafficking of Neurexin1α in mature neurons.

(a) Illustration of the strategy used during live-cell imaging experiments to label the axon. Representative image of a live DIV8 WT rat cortical neuron co-expressing SBP-GFP-Nrxn1α (grayscale and green) and streptavidin-KDEL immunostained for pan-Neurofascin (axon initial segment marker, grayscale and red).

(b and c) Live-cell imaging in DIV3 WT rat cortical neurons co-expressing SBP-GFP-Nrxn1α and streptavidin-KDEL. After 25–29 hr of expression neurons were imaged every 5 min for 2.5 hr. Biotin was added 10 min after the beginning of the imaging session. See also **Supplementary Movie 4.**

(b) Representative images of GFP-Nrxn1α endogenous fluorescence in dendrites and axons before (*t*0), 30, 60, 90 and 120 min after adding biotin. Red arrowheads indicate the axon and black arrows indicate GFP-Nrxn1α-positive puncta.

(c) Quantification of GFP-Nrxn1α fluorescence intensity in the soma, dendrites and axons (n = 9 neurons) in 2 independent experiments.

(d–h) After washing out BFA-mediated blocking of newly synthesized membrane protein transport through the secretory pathway, Nrxn1α is first inserted at the somatodendritic plasma membrane (BFA-mediated pulse-chase assay).

(e) DIV7, DIV9 WT mouse cortical neurons expressing extracellular HA-tagged Nrxn1α were treated with BFA 4 hr after transfection. Following 16 hr of treatment, BFA was washed out (*t*0) and neurons were fixed after different time points (1, 2 or 4 hr).

(d and f) High-zoom images of internal or surface HA-Nrxn1α in dendrites and axons. Neurons were first immunostained for surface HA-Nrxn1α (grayscale and green) under non-permeabilized conditions (f). After permeabilization, neurons were stained for internal HA-Nrxn1α (grayscale and green), MAP2 (blue) and Ankyrin-G (not shown) (d).

(g and h) Quantification of (d and f): internal and surface Nrxn1α fluorescence intensity in dendrites and axons relative to total levels in 3 independent experiments (n = 30 neurons for each group).

Graphs show mean ± SEM. Scale bars, 20 μm (a); 10 μm (b); 5 μm (f).

Supplementary Figure 3.

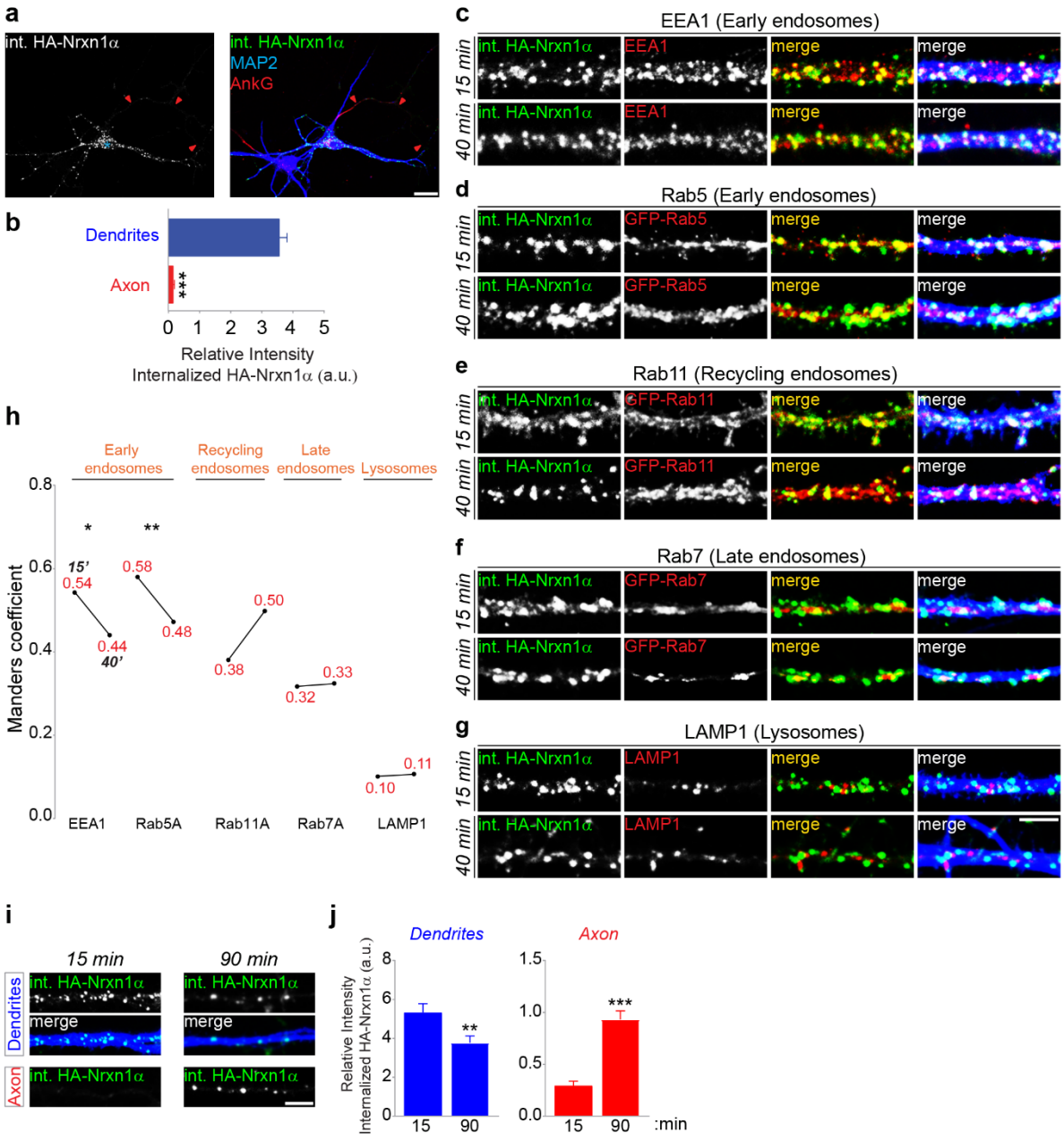

Supplementary Figure S3. Neurexin1α is internalized from the dendritic surface, incorporated into endosomes and transcytosed to the axon.

(a-j) Antibody pulse-chase experiments in DIV8–DIV11 WT mouse cortical neurons expressing extracellular HA-tagged Nrxn1α or co-expressing HA-Nrxn1α and GFP-tagged endosomal markers for 48 hr.

(a) Representative images of mouse cortical neurons pulse-chase for 15 min and immunostained for internalized HA-Nrxn1α (grayscale and green), MAP2 (blue) and Ankyrin-G (red). Red arrowheads indicate the axon and blue asterisk marks the cell body.

(b) Quantification of internalized Nrxn1α fluorescence intensity in dendrites and axons relative to total levels (n = 15 neurons). ***p < 0.001 (Mann-Whitney test, 3 independent experiments). Graph shows mean ± SEM.

(c–g) High-zoom images of dendritic segments from mouse cortical neurons pulse-chase for 15 min or 40 min and immunostained for internalized HA-Nrxn1α (grayscale and green), MAP2 (blue); EEA1 (early endosomal marker, in grayscale and red) (c), GFP-Rab5 (early endosomal marker, in grayscale and red) (d), GFP-Rab11 (recycling endosomal marker, in grayscale and red) (e), GFP-Rab7 (late endosomal marker, in grayscale and red) (f) or LAMP1 (lysosomal marker, in grayscale and red) (g).

(h) Quantification of the colocalization of internalized Nrxn1α with different endosomal or lysosomal markers expressed as Mander's coefficient (n = 15 neurons for each group). Graph shows mean. *p < 0.05; **p < 0.01 (Mann-Whitney test, 3 independent experiments).

(i) High-zoom images of dendritic or axonal segments from mouse cortical neurons pulse-chased for either 15 min or 90 min and labeled for internalized HA-Nrxn1α (grayscale and green), MAP2 (blue) and Ankyrin-G (not shown).

(j) Quantification of (i): internalized HA-Nrxn1α fluorescence intensity in axon and dendrites relative to total levels of internalized HA (n = 29 neurons for each group). Graphs show mean ± SEM. **p < 0.01; ***p < 0.001 (Mann-Whitney test, 3 independent cultures).

Scale bars, 20 µm (whole cell panels); 5 µm (high-zoom images).

Supplementary Figure 4.

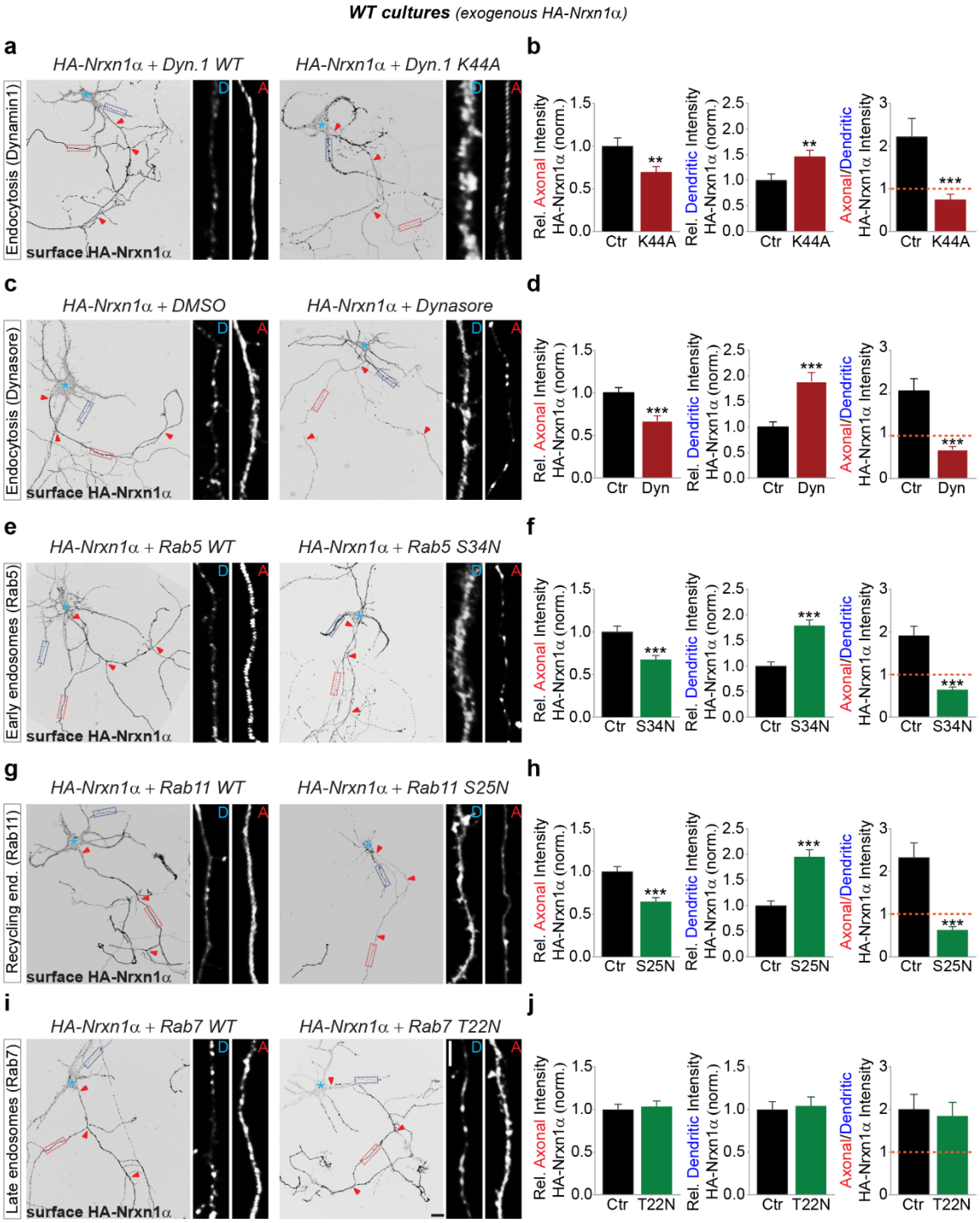

Supplementary Figure 4. Endocytosis and transport via endosomes are required to sustain axonal levels of Neurexin1α.

(a) Representative images of DIV8–DIV10 WT mouse cortical neurons co-expressing HA-Nrxn1α and GFP-tagged WT Dynamin1 (Ctr) or a dominant negative of GFP-Dynamin1 (K44A, to block Dynamin-

dependent endocytosis) for 48 hr. Neurons were immunostained for surface HA-Nrxn1α in grayscale; MAP2, Ankyrin-G and GFP (not shown). Red arrowheads indicate the axon and blue asterisk marks the cell body. High-zoom images of dendritic [D, dotted blue box] and axonal [A, dotted red box] Nrxn1α are shown next to the whole cell images.

(b) Quantification of (a): surface HA-Nrxn1α fluorescence intensity in axon and dendrites relative to total surface levels and normalized to cells expressing Dyn.1 WT and ratio of axonal/dendritic surface HA intensity. Ctr (n = 30 neurons); K44A (n = 30).

(c) Representative images of DIV8–DIV9 WT mouse cortical neurons expressing extracellular HA-tagged Nrxn1α and treated either with DMSO (vehicle, Ctr) or with Dynasore (Dyn) 30 hr after transfection. Neurons were immunostained 18 hr after treatment for surface HA-Nrxn1α (grayscale); MAP2 and Ankyrin-G (not shown).

(d) Quantification of (c);. Ctr (n = 30 neurons); Dyn (n = 27).

(e) Representative images of DIV8–DIV10 WT cortical neurons co-expressing HA-Nrxn1α and GFP-tagged WT Rab5 (Ctr) or a dominant negative of GFP-Rab5 (S34N, to prevent the formation of early endosomes) for 48 hr. Neurons were immunostained for surface HA-Nrxn1α (grayscale); MAP2, Ankyrin-G and GFP (not shown).

(f) Quantification of (e); Ctr (n = 29 neurons); S34N (n = 27).

(g) Representative images of DIV8–DIV10 WT cortical neurons co-expressing HA-Nrxn1α and GFP-tagged WT Rab11 (Ctr) or a dominant negative of GFP-Rab11 (S25N, to prevent the formation of recycling endosomes) for 48 hr. Neurons were immunostained for surface HA-Nrxn1α (grayscale); MAP2, Ankyrin-G and GFP (not shown).

(h) Quantification of (g); Ctr (n = 30 neurons); S25N (n = 27).

(i) Representative images of DIV8–DIV10 WT mouse cortical neurons co-expressing extracellular HA-tagged Nrxn1α and GFP-tagged WT Rab7 (Ctr) or a dominant negative of GFP-Rab7 (T22N, to prevent the formation of late endosomes) for 48 hr. Neurons were immunostained for surface HA-Nrxn1α (grayscale); MAP2, Ankyrin-G and GFP (not shown).

(j) Quantification of (i); Ctr (n = 30 neurons); T22N (n = 29).

Graphs show mean ± SEM. *p < 0.05; **p < 0.01; ***p < 0.001 (Mann-Whitney test, 3 independent cultures). Scale bars, 20 μm (whole cell panels); 5 μm (high-zoom images).

Supplementary Figure 5.

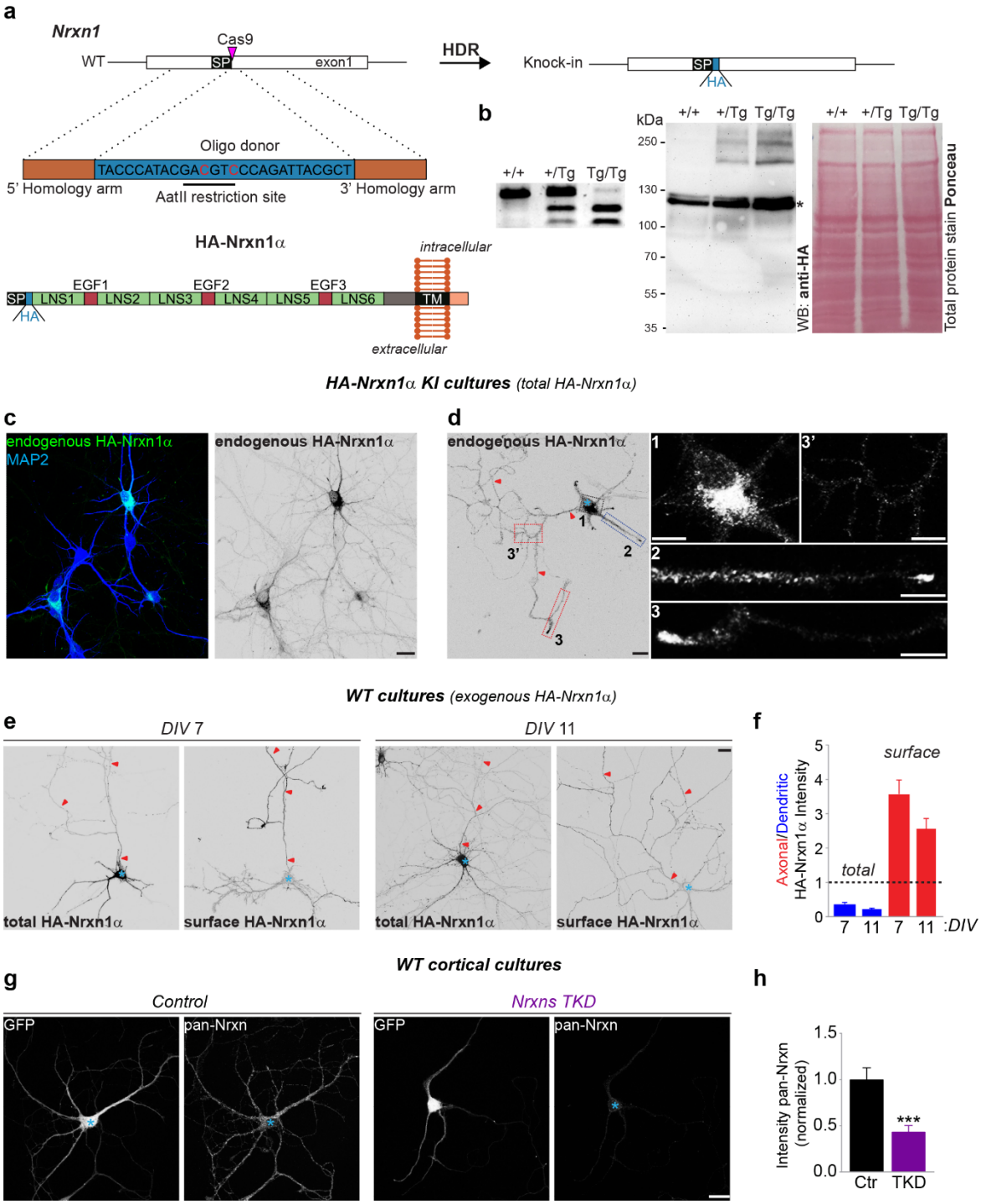

Supplementary Figure 5. Neurexin1α localizes to the somatodendritic and axonal compartment.

(a and b) *Nrxn1α*$^{HA/HA}$ knock-in (KI) mouse generation and validation.

(a) Orange boxes represent the left and right homologous arms. Blue box represents the single-strand DNA (ssDNA) donor oligonucleotide containing the HA-tag. CRISPR/Cas9-mediated homology directed repair

(HDR) allowed for precise HA-tagging of the *Nrxn1* locus right after the signal peptide (SP). An AatII restriction site was introduced in the DNA sequence coding for the HA-tag, by taking advantage of the redundancy of the genetic code, in order to facilitate the distinction between homozygous and heterozygous *Nrxn1α*$^{HA/HA}$ mice. Schematic representation of Nrxn1α protein domain organization is shown to illustrate the HA-tagging of HA-Nrxn1α right after the SP in the extracellular domain. Domain abbreviations: LNS, laminin/neurexin/sex hormone-binding globulin; EGF, epidermal growth factor-like; TM, transmembrane.

(b) Left panel: identification of WT (+/+), heterozygous (+/Tg) and homozygous (Tg/Tg) *Nrxn1α*$^{HA/HA}$ mice by generation of a PCR fragment of 499 bp followed by AatII-mediated restriction endonuclease reaction generating two DNA fragments of 312 bp and 187 bp. Right panels: detection of HA-Nrxn1α by western blot in cortical extracts prepared from adult *Nrxn1α*$^{HA/HA}$ KI mice (three months old). Total protein staining by using Ponceau method was used as loading control. Asterisk indicates an aspecific band.

(c and d) Representative images of permeabilized DIV7 *Nrxn1α*$^{HA/HA}$ mouse cortical neurons cultured together with WT mouse cortical neurons immunostained for HA-Nrxn1α (green and grayscale), MAP2 (blue) and Ankyrin-G (not shown). Red arrowheads indicate the axon and blue asterisk marks the cell body. High-zoom images of the subcellular distribution of endogenous HA-Nrxn1α: cell body (1), dendrites (2) and axon (3 and 3').

(e) Representative images of DIV7 and DIV11 WT mouse cortical neurons expressing extracellular HA-tagged Nrxn1α for 48 hr and immunostained for total or surface HA-Nrxn1α (grayscale); MAP2 and Ankyrin-G (not shown).

(f) Quantification of total and surface HA-Nrxn1α compartmentalized polarization: ratio of axonal/dendritic HA fluorescence intensity (3 independent experiments). total_DIV7 (n = 30 neurons); total_DIV11 (n = 30); surface_DIV7 (n = 30); surface_DIV11 (n = 29).

(g and h) Validation of anti-pan-Nrxn antibody.

(g) Representative images of DIV8, DIV10 WT mouse cortical neurons electroporated with L315 control construct (Control) or L315 Nrxn triple knockdown construct (Nrxns TKD)[1,2] immunostained for pan-Nrxn (grasycale) and GFP (grasycale). Blue asterisk marks the cell body.

(h) Quantification of (g): Nrxn fluorescence intensity normalized to cells expressing GFP (n = 45 neurons for each group). ***p < 0.001 (Mann-Whitney test, 3 independent experiments).

Graphs show mean ± SEM. Scale bars, 20 μm (whole cell panels); 10 μm (high-zoom images).

Supplementary Figure 6.

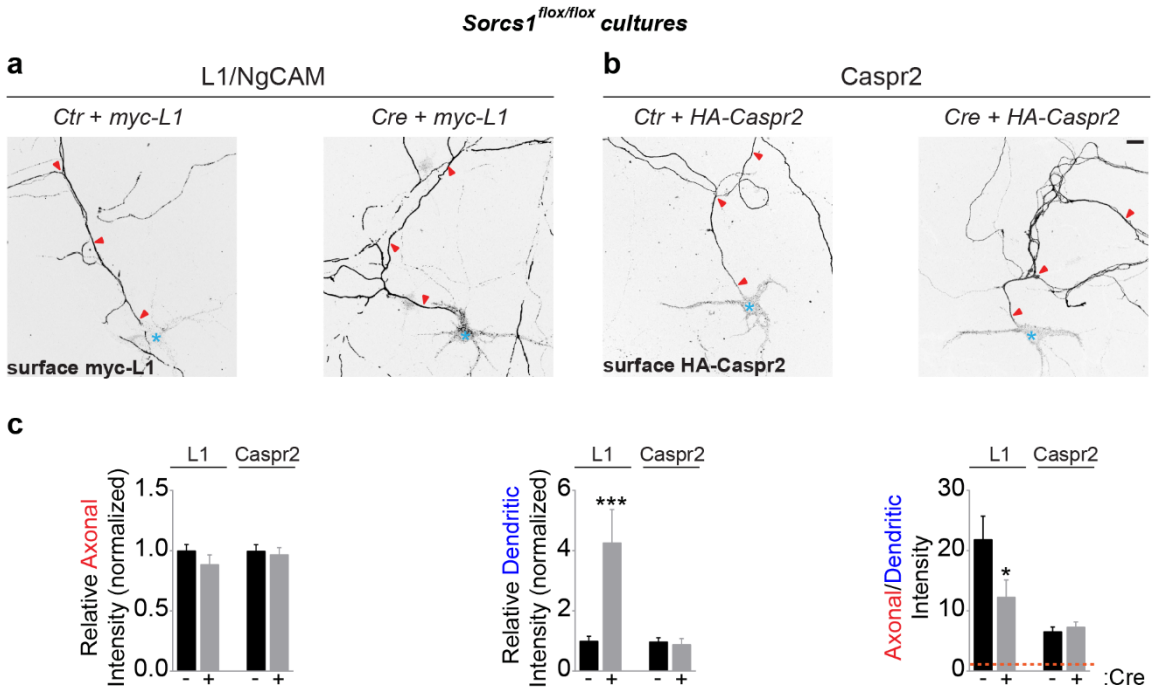

Supplementary Figure 6. Selective mis-sorting of transcytotic cargo in the absence of SorCS1.

(a and b) DIV8–DIV10 *Sorcs1*$^{flox/flox}$ mouse cortical neurons electroporated with EGFP (Ctr) or Cre-EGFP, and transfected with myc-L1 (a) or HA-Caspr2 (b), immunostained for surface myc-L1 or HA-Caspr2 in grasycale; MAP2, Ankyrin-G and GFP (not shown).

(c) Quantification of (a and b): surface L1 and Caspr2 fluorescence intensity in axon and dendrites relative to total surface levels and normalized to cells expressing EGFP and ratio of axonal/dendritic surface L1 and Caspr2 intensity. Ctr_L1 (n = 29 neurons); Cre_L1 (n = 26); Ctr_Caspr2 (n = 28); Cre_Caspr2. Graphs show mean ± SEM. *p < 0.05; **p < 0.01; ***p < 0.001 (Mann-Whitney test, at least 3 independent cultures). Scale bars, 20 µm.

Supplementary Figure 7.

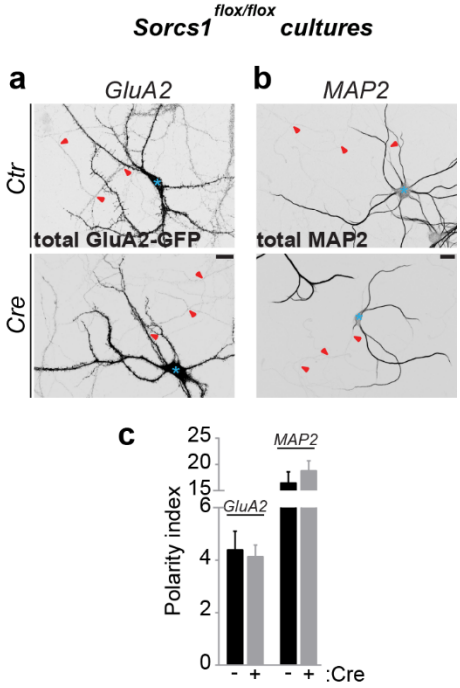

Supplementary Figure 7. Sorting of somatodendritic cargo is not affected by loss of SorCS1.

(a) Representative images of DIV14 *Sorcs1*$^{flox/flox}$ cortical neurons co-expressing GFP-GluA2 and an empty vector (Ctr) or GFP-GluA2 and Cre-myc (Cre) for 7 d. Neurons were immunostained for GFP-GluA2 (grayscale); MAP2, Ankyrin-G and myc (not shown). Red arrowheads indicate the axon and blue asterisk marks the cell body. Scale bars, 20 µm.

(b) Representative images of DIV10 mouse *Sorcs1*$^{flox/flox}$ cortical neurons electroporated with EGFP (Ctr) or Cre-EGFP (Cre) immunostained for MAP2 (grayscale); Ankyrin-G and GFP (not shown).

(c) Quantification of (a and b): dendritic versus axonal distribution (D:A – polarity index) of GluA2 or MAP2 in WT and *Sorcs1* KO cells (at least 1 independent experiment). GluA2_Ctr (n = 9 neurons); GluA2_Cre (n = 9); MAP2_Ctr (n = 18); MAP2_Cre (n = 20). Graph shows mean ± SEM.

Supplementary Figure 8.

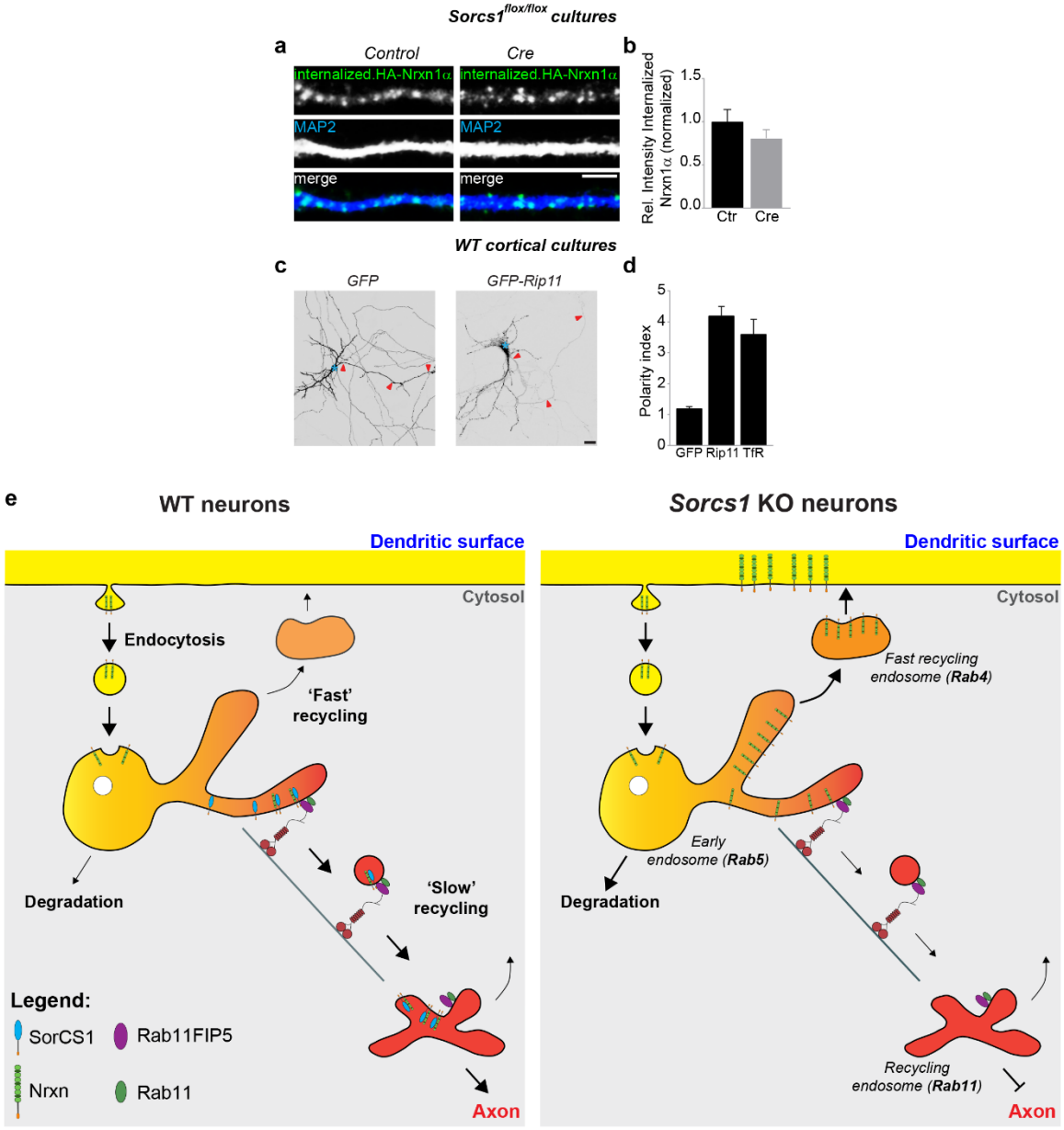

Supplementary Figure 8. Internalization of Neurexin1α is not affected in *Sorcs1* KO cells; and Rab11FIP5/Rip11, a new binding partner of SorCS1, localizes to the somatodendritic compartment. (a) High-zoom images of dendritic internalized Nrxn1α from DIV8, DIV10 *Sorcs1*$^{flox/flox}$ cortical neurons electroporated with EGFP (Control) or Cre-EGFP (Cre) and transfected with extracellular HA-tagged Nrxn1α for 48 hr. Live neurons were incubated with an anti-HA antibody and pulse-chased for 20 min. Neurons were immunostained for internalized HA-Nrxn1α (grayscale and green), MAP2 (grayscale and blue); surface HA-Nrxn1α and GFP (not shown). Scale bar, 5 μm.

(b) Quantification of (a): internalized Nrxn1α fluorescence intensity relative to total levels and normalized to cells expressing GFP (3 independent experiments). Control (n = 30 neurons); Cre (n = 28). Graph shows mean ± SEM.

(c) Representative images of DIV9–DIV10 WT mouse cortical neurons expressing EGFP or EGFP-Rip11 for 48 hr and immunostained for GFP (grayscale); MAP2 and Ankyrin-G (not shown). Red arrowheads indicate the axon and blue asterisk marks the cell body. Scale bar, 20 μm.

(d) Quantification of (c): dendritic versus axonal distribution (D:A – polarity index) of GFP (n = 20 neurons), Rip11 (n = 19) and TfR (n = 16) from 2 independent experiments. Graph shows mean ± SEM.

(e) Model for SorCS1-mediated sorting of Nrxn. Upon internalization from the dendritic plasma membrane, cargo proteins are incorporated into small carrier vesicles that fuse with existing early endosomes (EEs) (Rab5- and EEA1-positive). From EEs, cargo can recycle back to the plasma membrane via fast recycling endosomes (REs) (Rab4-positive). Alternatively, cargo can be sorted into multivesicular bodies (MVBs) or Rab11-positive REs. MVBs carry cargo to late endosomes (LEs; Rab7-positive)/lysosomes for degradation. Cargo destined for either axon or dendrites is sorted via Rab11-REs and transported to its respective final destination[3,4]. SorCS1/Rab11FIP5 sorting complex localizes to EEs and sorts newly internalized Nrxn into cytoskeleton-associated vesicles that carry cargo from EEs to Rab11-REs. Nrxn-containing Rab11-REs are subsequently transcytosed from dendrites to the axon. In *Sorcs*1 KO cells, Nrxn is not sorted to Rab11-REs, accumulating in EEs and mis-trafficking to Rab4-REs. Consequently, axonal surface levels of Nrxn are decreased and dendritic surface levels are increased, which is likely due to decreased sorting of Nrxn to Rab11-REs and increased recycling of Nrxn from Rab4-REs back to the dendritic plasma membrane, respectively.

Supplementary Figure 9.

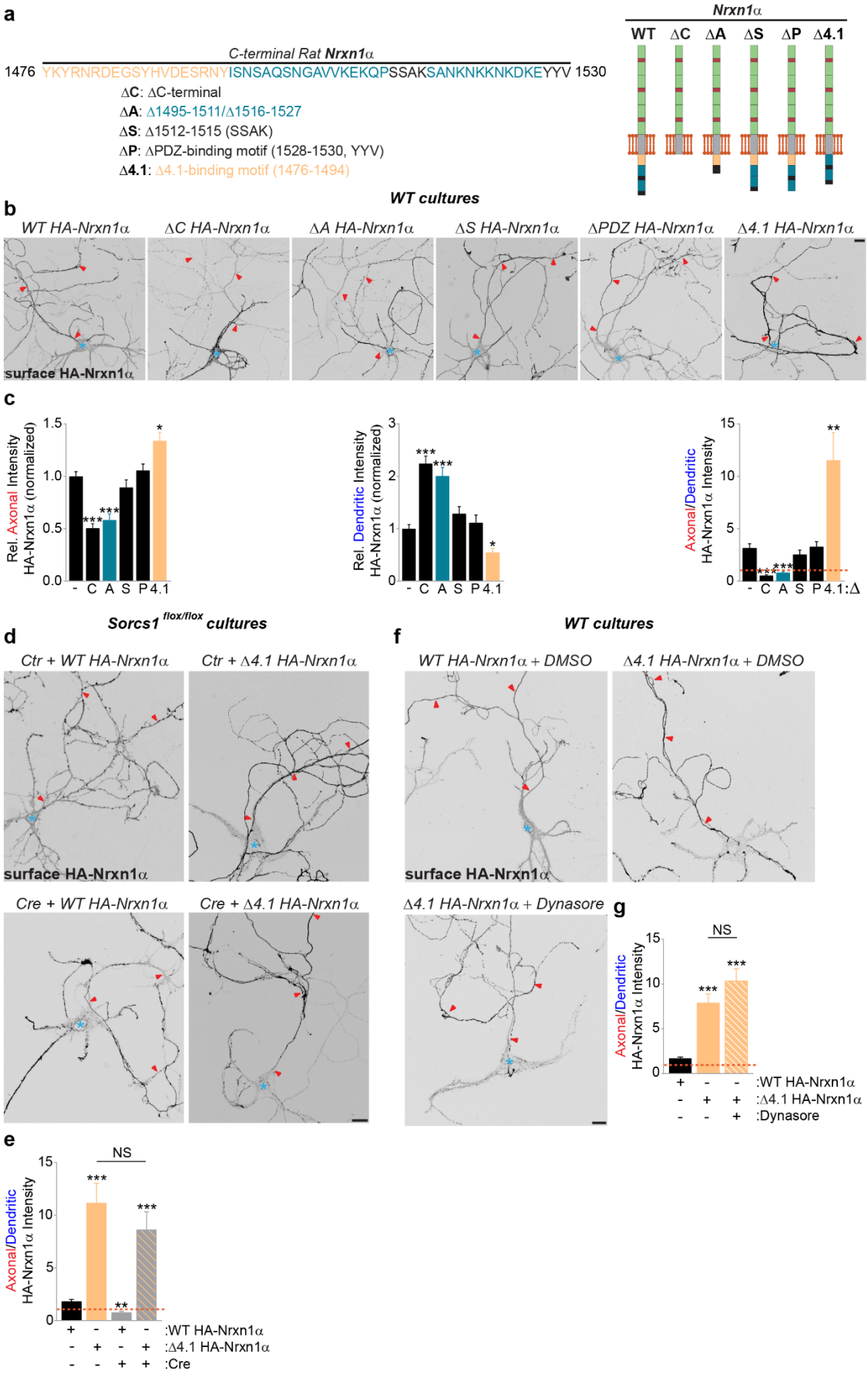

Supplementary Figure 9. Neurexin1α lacking the 4.1-binding motif in the cytoplasmic domain traffics to the axon in a SorCS1- and endocytosis-independent manner.

(a) Schematic representation of WT and C-terminal mutants of rat Nrxn1α. Different deletion mutants of Nrxn1α C-terminal were designed: deletion mutant of the entire C-terminal (ΔC), deletion mutant spanning the regions 1495–1511 and 1516–1527 (ΔA), deletion mutant lacking a putative phosphorylation site in serine 1513 (ΔS), deletion mutant lacking the PDZ-binding motif (ΔP) and deletion mutant lacking the 4.1-binding motif (Δ4.1). Red arrowheads indicate the axon and blue asterisk marks the cell body.

(b) Representative images of DIV8–DIV10 WT mouse cortical neurons expressing extracellular HA-tagged WT-Nrxn1α and C-terminal deletions mutants of Nrxn1α for 48 hr and immunostained for surface HA-Nrxn1α (grayscale); MAP2 and Ankyrin-G (not shown).

(c) Quantification of (b): surface HA-Nrxn1α fluorescence intensity in axon and dendrites relative to total surface levels and normalized to cells expressing WT-Nrxn1α and ratio of axonal/dendritic surface HA intensity. WT (n = 40 neurons); ΔC (n = 30); ΔA (n = 30); ΔS (n = 29), ΔP (n = 30); Δ4.1 (n = 30). *p < 0.05; **p < 0.01; ***p < 0.001 (Kruskal-Wallis test followed by Dunn's multiple comparisons test, at least 3 independent experiments).

(d) Representative images of DIV8–DIV10 mouse *Sorcs1*$^{flox/flox}$ cortical neurons electroporated with EGFP (Ctr) or Cre-EGFP (Cre) and transfected for 48 hr with extracellular HA-tagged WT Nrxn1α or 4.1 C-terminal deletion mutant. Neurons were immunostained for surface HA-Nrxn1α (grayscale); MAP2, Ankyrin-G and GFP (not shown).

(e) Quantification of HA-Nrxn1α surface polarization: ratio of axonal/dendritic surface HA fluorescence intensity. Ctr_WT (n = 46 neurons); Ctr_Δ4.1 (n = 25); Cre_WT (n = 30); Cre_Δ4.1 (n = 27). NS, non-significant; *p < 0.05; **p < 0.01; ***p < 0.001 (Kruskal-Wallis test followed by Dunn's multiple comparisons test, at least 3 independent experiments).

(f) Representative images of DIV8–DIV10 WT mouse cortical neurons expressing extracellular HA-tagged WT Nrxn1α and treated with DMSO (vehicle) 30 hr after transfection, expressing 4.1-binding motif deletion mutant (Δ4.1) and treated with DMSO or expressing Δ4.1 and treated with Dynasore. Neurons were immunostained 18 hr after treatment for surface HA-Nrxn1α (grayscale); MAP2 and Ankyrin-G (not shown).

(g) Quantification of HA-Nrxn1α surface polarization: ratio of axonal/dendritic surface HA fluorescence intensity. WT_DMSO (n = 40 neurons); Δ4.1_DMSO (n = 40); Δ4.1_Dynasore (n = 28). NS, non-significant; ***p < 0.001 (Kruskal-Wallis test followed by Dunn's multiple comparisons test, at least 3 independent experiments).

Graphs show mean ± SEM. Scale bars, 20 μm.

Supplementary Figure 10.

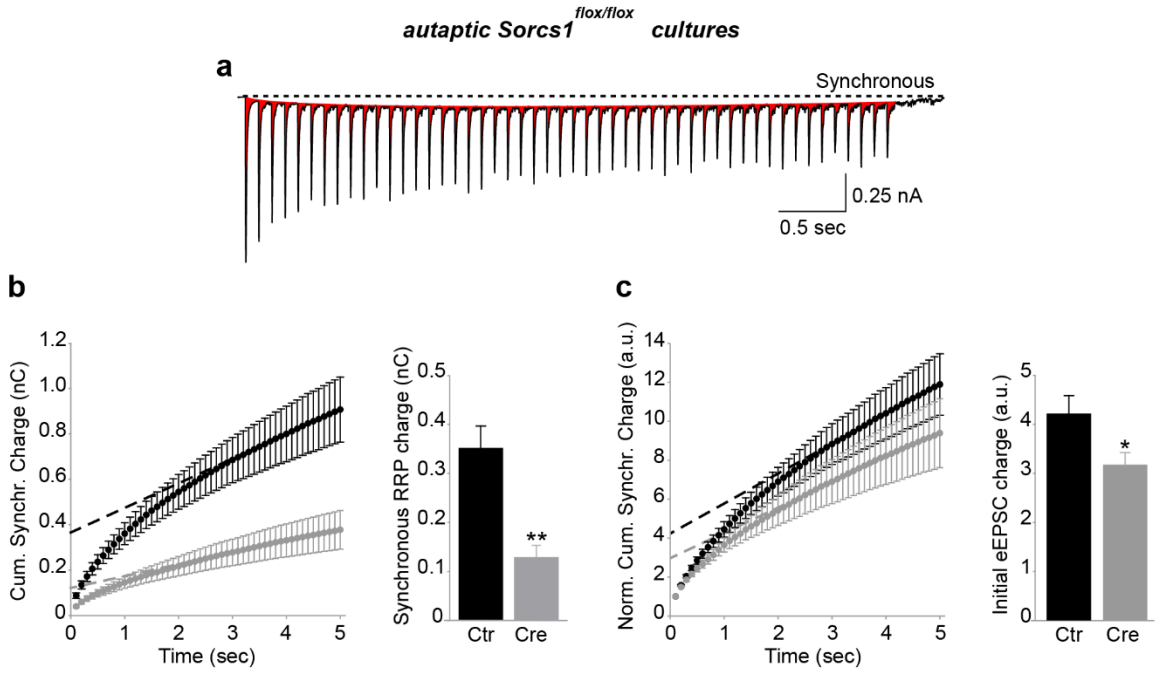

Supplementary Figure 10. Defects in synaptic transmission in *Sorcs1* KO neurons.

(a) Estimation of the synchronous charge during 10 Hz train stimulations, shown in red.

(b) Estimation of the RRP size used during neuronal activity by back-extrapolating a linear fit of the steady state current towards the ordinate axis intercept, which represents the initial RRP size before train stimulations (10 Hz)[5]. RRP size of active synapses was reduced in DIV14–DIV16 *Sorcs1* KO neurons. Control (n = 18 neurons); Cre (n = 13). **p < 0.01 (Mann-Whitney test, 3 independent experiments).

(c) Kinetics of activity dependent depletion of the RRP, using repetitive train stimulations (10 Hz). We normalized eEPSC synchronous charge – to assess release kinetics independent of the difference in RRP pool size – and calculated the initial eEPSC charge before stimulation. DIV14–DIV16 *Sorcs1* KO neurons showed a smaller initial eEPSC charge, suggesting a reduced efficacy of calcium dependent synaptic vesicle release during repetitive stimulation. Control (n = 18 neurons); Cre (n = 13). *p < 0.05 (Mann-Whitney test, 3 independent experiments).

Graphs show mean ± SEM.

SUPPLEMENTARY TABLES

Supplementary Table 1: Plasmids list

Plasmids		
pIRESneo3-Str-KDEL_SBP-EGFP-GPI	Addgene plasmid[6]	Cat #65294
pIRESneo3-Str-KDEL_SBP-EGFP-Nrxn1α	This paper	N/A
pIRESneo3-Str-KDEL_TfR-SBP-EGFP	[7]	N/A
pCAG-HA-Nrxn1α(-SS4)	[8]	N/A
pCAG-HA-Nrxn1α(-SS4)Δ4.1	This paper	N/A
pCAG-HA-Nrxn1α(-SS4)ΔC-terminal	This paper	N/A
pCAG-HA-Nrxn1α(-SS4)Δ1495-1511/Δ1495-1511	This paper	N/A
pCAG-HA-Nrxn1α(-SS4)ΔPDZ binding motif	This paper	N/A
pCAG-HA-Nrxn1α(-SS4)Δ1512-1515	This paper	N/A
pFUGW-EGFP_T2A_HA-Nrxn1α(-SS4)	This paper	N/A
pFUGW-EGFP_T2A_HA-Nrxn1α(-SS4)ΔN-terminal	This paper	N/A
pcDNA4-mSorCS1cβ-myc	[9]	N/A
pcDNA4-mSorCS1cβ-myc Y1132A	This paper	N/A
pcDNA3.1-HA-mSorCS1cβ	This paper	N/A
pcDNA3.1-HA-mSorCS1cβ Y1132A	This paper	N/A
pBOS-EGFP	[10]	N/A
pEGFP-N1	Clontech	Cat #6085-1
pcDNA3.1(-)	Thermo Fisher Scientific	Cat #V79520
pcDNA3.1(+)	Thermo Fisher Scientific	Cat #V79020
pFUGW	[11]	N/A
pFUGW-mCherry	This paper	N/A
pFUGW-Cre_T2A_mCherry	This paper	N/A
pFUGW-Cre_T2A_mCherry_T2A_Nrxn1α WT	This paper	N/A
pFUGW-Cre_T2A_mCherry_T2A_Nrxn1αΔ4.1	This paper	N/A
pFUGW-Cre-EGFP	This paper	N/A
pFUGW-Cre-EGFP_T2A_SorCS1 WT	This paper	N/A
pFUGW-Cre-EGFP_T2A_SorCS1 Y1132A	This paper	N/A
FCK(0.4)GW	[11]	N/A
FCK(0.4)GW-Cre-EGFP	This paper	N/A
pCAG-Cre-myc	Anirvan Ghosh (Biogen, USA)	N/A
pEGFP-N3-Rip11	[12]	N/A
pEGFP-C1-Rip11(490–653)	[12]	N/A
extracellularly myc-tagged L1	[13]	N/A
pcDNA3-HA-Caspr2	[14]	N/A
FLAG-tagged Nlgn1	Davide Comoletti (Rutgers University, USA)	N/A
pEGFP-N1-NGL-3	[15]	N/A
GFP-tagged GluA2	Anirvan Ghosh (Biogen, USA)	N/A
GFP-tagged TfR	Juan S. Bonifacino (National Institute of Health, USA)	N/A
L315 control construct	[1]	N/A
L315 Nrxn triple knockdown construct	[1]	N/A
GFP-tagged Dynamin1 WT	[16]	N/A
GFP-tagged Dynamin1 WT K44A	[16]	N/A
GFP-tagged Rab5 WT	Marino Zerial (Max Planck Institute, Dresden, Germany)	N/A
GFP-tagged Rab5 S34N	Marino Zerial (Max Planck Institute, Dresden, Germany)	N/A
GFP-tagged Rab11 WT	Casper Hoogenraad (Utrecht University, The Netherlands)	N/A
GFP-tagged Rab11 S25N	Casper Hoogenraad (Utrecht University, The Netherlands)	N/A
GFP-tagged Rab4 WT	Casper Hoogenraad (Utrecht University, The Netherlands)	N/A
GFP-tagged Rab7 WT	Casper Hoogenraad (Utrecht University, The Netherlands)	N/A
GFP-tagged Rab7 T22N	This paper	N/A

Supplementary Table 2: Antibodies list

Antibodies		
Anti-MAP2, chicken	Abcam	Cat #ab5392
Anti-Ankyrin-G, mouse	NeuroMab	Cat #73-146
Anti-Ankyrin-G, goat	Santa Cruz Biotechnology	Cat #sc-31778
Anti-GFP, chicken	Aves	Cat #GFP-1010
Anti-GFP, rabbit	Millipore	Cat #AB3080
Anti-GFP, mouse	Santa Cruz Biotechnology	Cat #sc-9996
Anti-pan-Neurofascin, mouse	NeuroMab	Cat #75-172
Anti-pan-Neurexin, rabbit	[17]	N/A
Anti-EEA1, rabbit	Sigma-Aldrich	Cat #E4156
Anti-LAMP1, rat	Developmental Studies Hybridoma Bank	Cat #1D4B
Anti-HA, mouse	Covance	Cat #MMS-101P
Anti-HA, mouse	Biolegend	Cat #901502
Anti-HA, rabbit	Sigma-Aldrich	Cat #H6908
Anti-HA, rabbit	Cell Signaling Technology	Cat #3724
Anti-Rip11, rabbit	[18]	N/A
Anti-myc, mouse	Santa Cruz Biotechnology	Cat #sc-40
Anti-synapsin1, rabbit	Millipore	Cat #AB1543P
CF405M, anti-chicken	Sigma-Aldrich	Cat #SAB4600466
CF405M, anti-goat	Biotium	Cat #20398
Alexa 488, anti-chicken	Invitrogen	Cat #A11039
Alexa 488, anti-mouse	Invitrogen	Cat #A21202
Alexa 488, anti-rabbit	Invitrogen	Cat #A21206
Alexa 488, anti-goat	Invitrogen	Cat #A11055
Alexa 555, anti-chicken	Invitrogen	Cat #A21437
Alexa 555, anti-mouse	Invitrogen	Cat #A31570
Alexa 555, anti-rabbit	Invitrogen	Cat #A31572
Alexa 555, anti-goat	Invitrogen	Cat #A21432
Alexa 647, anti-chicken	Jackson ImmunoResearch	Cat #703-605-155
Alexa 647, anti-mouse	Invitrogen	Cat #A31571
Alexa 647, anti-rabbit	Invitrogen	Cat #A31573
Fab fragment, anti-mouse	Jackson ImmunoResearch	Cat #715-007-003

METHODS

Animals

All animal procedures were approved by the Institutional Animal Care and Research Advisory Committee of the KU Leuven (ECD P015/2013 and ECD P214/2017) and were performed in accordance with the Animal Welfare Committee guidelines of the KU Leuven, Belgium. The health and welfare of the animals was supervised by a designated veterinarian. The KU Leuven animal facilities comply with all appropriate standards (cages, space per animal, temperature, light, humidity, food, water), and all cages are enriched with materials that allow the animals to exert their natural behavior. Wistar rats were obtained from Janvier Labs. CD-1 and C57BL/6J mice were obtained KU Leuven Mouse Facility. C57BL/6J *Sorcs1*$^{flox/flox}$ mice were previously described[9] and kindly provided by Alan D. Attie (University of Wisconsin-Madison, USA). C57BL/6J *Nrxn1α*$^{HA/HA}$ and C57BL/6J *Sorcs1*$^{HA/HA}$ knock-in (KI) mice were generated by CRISPR/Cas9-mediated homology directed repair (HDR) targeting the mouse *Nrxn1* locus at exon 2 and *Sorcs1* locus at exon 1. C57BL/6J *Sorcs1*$^{HA/HA}$ was commercially purchased from Cyagen, whereas C57BL/6J *Nrxn1α*$^{HA/HA}$ was generated in-house at the Mutamouse core facility (KU Leuven/VIB). To generate *Nrxn1α*$^{HA/HA}$ KI, CRISPR/Cas9 components were microinjected in zygotes as ribonucleoproteins (RNPs) composed of: crRNA (guide RNA sequence: 5'-TCCACTGGCCCTCGGCGCCC-3') (IDT), tracrRNA (IDT, Cat #1072534), ssODN (oligo DNA donor sequence: 5'-TGCTGTCTCCTCTGCCTGTCGCTGCTGCTGCTGGGCTGCTGGGCAGAGCTGGGCAGCGGGTACCCATACGAC GTCCCAGATTACGCTCTGGAGTTTCCGGGCGCCGAGGGCCAGTGGACGCGCTTCCCCAAGTGGAACGCGTGC TGC-3') (IDT) and Cas9 (IDT, Cat #1074182). To generate *Sorcs1*$^{HA/HA}$ KI the donor DNA (5'-GTCGGAGCCGCCGGGACATGCTAAAGGATGGAGGGCAGCAGGGGCTTGGGACTGGCGCATACCCATACGATG TTCCAGATTACGCTCGGGACCCGGACAAAGCCACCCGCTTCCGGATGGAGGAGCTGAGACTGACCAGCACCAC A-3') and guide RNA (5'-TGGGACTGGCGCACGGGACCCGG-3') were used. Insertion of the HA epitope tag was validated by western blot. To mitigate possible CRISPR/Cas9-mediated off-targets C57BL/6J *Nrxn1α*$^{HA/HA}$ and C57BL/6J *Sorcs1*$^{HA/HA}$ mice were backcrossed to WT C57BL/6J. C57BL/6J *Nrxn1α*$^{HA/HA}$ and C57BL/6J *Sorcs1*$^{HA/HA}$ mice are fertile and viable.

Cell Lines

HEK293T-17 human embryonic kidney cells (available source material information: fetus) were obtained from American Type Culture Collection (ATCC, Cat #CRL-11268). HEK293T-17 cells were grown in DMEM (Thermo Fisher Scientific, Cat #11965092) supplemented with 10% (vol/vol) FBS (Thermo Fisher Scientific, Cat #10270106) and 1% (vol/vol) penicillin/streptomycin (Thermo Fisher Scientific, Cat #15140122).

Neuronal Cultures

Primary neuronal cultures for imaging

Neurons were cultured from E18-E19 Wistar rat embryos (Janvier labs) (cortical), from E18–E19 C57BL/6J mice embryos (cortical and hippocampal), from E18–E19 C57BL/6J *Sorcs1*$^{flox/flox}$ mice (cortical), from E18–E19 C57BL/6J *Sorcs1*$^{HA/HA}$ mice (cortical) and E18–E19 C57BL/6J *Nrxn1α*$^{HA/HA}$ mice (cortical), as previously described[19]. Briefly, dissected hippocampi and cortices were incubated with trypsin [0.25% (vol/vol), 15 min, 37 °C] (Thermo Fisher

Scientific, Cat #15090046) in HBSS (Thermo Fisher Scientific, Cat #14175095) supplemented with 10 mM HEPES (Thermo Fisher Scientific, Cat #15630080). After trypsin incubation, hippocampi and cortices were washed with MEM (Thermo Fisher Scientific, Cat #11095080) supplemented with 10% (v/v) horse serum (Thermo Fisher Scientific, Cat #26050088) and 0.6% (wt/vol) glucose (MEM-horse serum medium) three times. The cells were mechanically dissociated by repeatedly pipetting the tissue up and down in a flame-polished Pasteur pipette, and then plated on poly-D-lysine (Millipore, Cat #A-003-E) and laminin (Sigma-Aldrich, Cat #L2020) coated glass coverslips (Glaswarenfabrik Karl Hecht, Cat #41001118) in 60 mm culture dishes (final density: 4 x 10^5–7 x 10^5 cells per dish), containing MEM-horse serum medium. Once neurons attached to the substrate, after 2–4 hr, the coverslips were flipped over an astroglial feeder layer in 60-mm culture dishes containing neuronal culture medium: Neurobasal medium (Thermo Fisher Scientific, Cat #21103049) supplemented with B27 (1:50 dilution; Thermo Fisher Scientific, Cat #17504044), 12 mM glucose, glutamax (1:400 dilution; Thermo Fisher Scientific, Cat #35050061), penicillin/streptomycin (1:500 dilution; Thermo Fisher Scientific, Cat #15140122), 25 µM β-mercaptoethanol, and 20 µg/mL insulin (Sigma-Aldrich, Cat #I9278). Neurons grew face down over the feeder layer but were kept separate from the glia by wax dots on the neuronal side of the coverslips. To prevent overgrowth of glia, neuron cultures were treated with 10 µM 5-Fluoro-2′-deoxyuridine (Sigma-Aldrich, Cat #F0503) after 3 d. Cultures were maintained in a humidified incubator of 5% (vol/vol) CO_2/95% (vol/vol) air at 37 °C, feeding the cells once per week by replacing one-third of the medium in the dish. Cortical neurons from C57BL/6J and C57BL/6J *Sorcs1*$^{flox/flox}$ mice were electroporated with DNA just before plating using an AMAXA Nucleofector kit (Lonza, Cat #VPG-1001). Cortical neurons from C57BL/6J *Sorcs1*$^{flox/flox}$ mice were transfected at DIV7 using Effectene (Qiagen, Cat #301425). Rat cortical neurons, and neurons from C57BL/6J (cortical and hippocampal), C57BL/6J *Sorcs1*$^{flox/flox}$ (cortical) and C57BL/6J *Nrxn1α*$^{HA/HA}$ (cortical) mice were transfected at DIV6–DIV8 using the calcium phosphate method. Mouse cortical neurons from C57BL/6J *Nrxn1α*$^{HA/HA}$ and C57BL/6J *Sorcs1*$^{HA/HA}$ were mixed with WT cortical neurons from C57BL/6J mice which allowed for the reliable immunodetection of endogenous HA-Nrxn1α and HA-SorCS1 with confidence.

Co-culture assays were performed as previously described[10]. Briefly, HEK293T cells grown in DMEM (Thermo Fisher Scientific, Cat #11965092) supplemented with 10% (vol/vol) FBS (Thermo Fisher Scientific, Cat #10270106) and 1% (vol/vol) penicillin/streptomycin (Thermo Fisher Scientific, Cat #15140122), were transfected with FLAG-tagged Nlgn1 or GFP-tagged NGL-3 using Fugene6 (Promega, Cat #E2691). Transfected HEK293T cells were mechanically dissociated 24 hr after transfection and co-cultured with DIV10 cortical neurons prepared from C57BL/6J *Sorcs1*$^{flox/flox}$ mice for 16 hr.

Primary autaptic cortical cultures for electrophysiology

For electrophysiology, we used isolated cortical neurons on astrocyte microislands[20]. In short, cortices were dissected from embryonic day 18 C57BL/6J *Sorcs1*$^{flox/flox}$ or C57BL/6J mice and collected in HBSS (Thermo Fisher Scientific, Cat #14175095) supplemented with 10 mM HEPES (Thermo Fisher Scientific, Cat #15630080). Cortical pieces were incubated for 15 min in HBSS supplemented with tripsin 0.25% (vol/vol) (Thermo Fisher Scientific, Cat #15090046) and 10 mM HEPES for 15 min at 37 °C. After trypsin blocking and washing with MEM (Thermo Fisher Scientific, Cat #11095080) supplemented with 10% (v/v) horse serum (Thermo Fisher Scientific, Cat #26050088) and 0.6% (wt/vol) glucose; neurons were dissociated, counted and plated in Neurobasal medium (Thermo Fisher Scientific, Cat #21103049) supplemented with B27 (1:50 dilution; Thermo Fisher Scientific, Cat #17504044), 12 mM glucose, glutamax (1:400 dilution; Thermo Fisher Scientific, Cat #35050061), penicillin/streptomycin (1:500 dilution; Thermo

Fisher Scientific, Cat #15140122) and 25 µM β-mercaptoethanol. Dissociated neurons were electroporated (*Sorcs1*$^{flox/flox}$: EGFP or Cre-EGFP; C57BL/6J: L315 control construct or L315 Nrxn triple knockdown construct) just before plating using AMAXA Nucleofector kit (Lonza, Cat #VPG-1001) and plated at 2500/cm^2 on micro islands of mouse (CD-1) glia. Glial islands were obtained by first coating glass coverslips with 0.15% (wt/vol) agarose. After drying and UV sterilization (30 min), customized stamps were used to create dots (islands, diameter 200–250 µm) using a substrate mixture containing 0.25 mg/mL rat tail collagen (Corning, Cat #354236) and 0.4 mg/mL poly-D-lysine (Sigma-Aldrich, Cat #P7405) dissolved in 17 mM acetic acid. After drying/UV treatment of the islands, ~25000 astrocytes were plated per 30 mm glass coverslip in 6-well plates and allowed to form micro-dot islands in DMEM (Thermo Fisher Scientific, Cat #11965092) supplemented with 10% (vol/vol) FBS (Thermo Fisher Scientific, Cat #10270106) for 3–5 d.

Plasmids

Constructs were all generated using the Gibson Assembly Cloning Kit (New England Biolabs, Cat #E5510S) by inserting the different DNA fragments (PCR-generated, gBlocks or ultramers) in the different final vectors digested with the respective restriction enzymes. For pFUGW-mCherry, pFUGW-Cre_T2A_mCherry, pFUGW-Cre_T2A_mCherry_T2A_Nrxn1α(-SS4)WT, pFUGW-Cre_T2A_mCherry_T2A_Nrxn1α(-SS4)Δ4.1, pFUGW-Cre-EGFP, pFUGW-Cre-EGFP_T2A_SorCS1WT, pFUGW-Cre-EGFP_T2A_SorCS1Y1132A, pFUGW-EGFP_T2A_HA-Nrxn1α(-SS4) and pFUGW-EGFP_T2A_HA-Nrxn1α(-SS4)ΔN-terminal (remaining N-terminal consists of HA epitope tag and 5 amino acids before the transmembrane region) PCR fragments were inserted into pFUGW vector[11] digested with AgeI and EcoRI. For pcDNA3.1-HA-SorCS1cβ a PCR fragment was inserted into pcDNA3.1(+) (Thermo Fisher Scientific, Cat #V79020) digested with EcoRI. For FCK(0.4)GW-Cre-EGFP a PCR fragment was inserted into FCK(0.4)GW vector[11] digested with AgeI and EcoRI. For pIRESneo3-Str-KDEL_SBP-EGFP-Nrxn1α a PCR fragment was inserted into pIRESneo3-Str-KDEL_SBP-EGFP-GPI (kindly provided by Franck Perez, Institute Curie, France; Addgene plasmid #65294; RRID: Addgene_65294) digested with FseI and PacI. To generate pCAG-HA-Nrxn1α(-SS4)Δ4.1, pCAG-HA-Nrxn1α(-SS4)ΔC-terminal, pCAG-HA-Nrxn1α(-SS4)Δ1495-1511/Δ1495-1511, pCAG-HA-Nrxn1α(-SS4)ΔPDZ binding motif and pCAG-HA-Nrxn1α(-SS4)Δ1512-1515 gBlocks or ultramers containing the different deletions of Nrxn1α C-terminal were inserted into pCAG-HA-Nrxn1α(-SS4) (kindly provided by Peter Scheiffele, University of Basel, Switzerland) digested with Bsp147I and SmaI. pcDNA4-SorCS1cβ-myc Y1132A, pcDNA3.1-HA-SorCS1cβ Y1132A and GFP-tagged Rab7 T22N were generated by *in vitro* mutagenesis using the QuikChange II Site-Directed Mutagenesis Kit (Agilent, Cat #200522) from pcDNA4-SorCS1cβ-myc (kindly provided by Alan D. Attie, University of Wisconsin-Madison, USA), pcDNA3.1-HA-SorCS1cβ and GFP-tagged Rab7 WT (kindly provided by Casper Hoogenraad, Utrecht University, The Netherlands), respectively. The following constructs were kindly provided by: pIRESneo3-Str-KDEL_TfR-SBP-EGFP and GFP-tagged TfR (Juan S. Bonifacino, National Institute of Health, USA); pCAG-Cre-myc and GFP-tagged GluA2 (Anirvan Ghosh, Biogen, USA); pEGFP-N3-Rip11 and pEGFP-C1-Rip11(490–653) (Rytis Prekeris, University of Colorado, USA); GFP-tagged Rab11 WT, GFP-tagged Rab11 S25N and GFP-tagged Rab4 WT (Casper Hoogenraad, Utrecht University, The Netherlands); GFP-tagged Rab5 WT and GFP-tagged Rab5 S34N (Ragna Sannerud, KU Leuven, Belgium); GFP-tagged Dynamin1 WT, GFP-tagged Dynamin1 WT K44A and pcDNA3-HA-Caspr2 (Catherine Faivre-Sarrailh, Aix-Marseille University, France); L315 control and L315 Nrxns TKD (Thomas C. Südhof, Stanford University, USA); FLAG-tagged Nlgn1 (Davide Comoletti, Rutgers University, USA); pEGFP-N1-NGL-3 (Eunjoon Kim, Korea Advanced Institute of Science

and Technology, South Korea); and myc-tagged L1 (Dan P. Felsenfeld, CHDI Foundation, USA). All DNA constructs used in this study were verified by sequencing.

Neuron Transfection

Rat cortical neurons (live-cell imaging experiments), and neurons from C57BL/6J (cortical and hippocampal), C57BL/6J *Sorcs1*$^{flox/flox}$ (cortical) and C57BL/6J *Nrxn1α*$^{HA/HA}$ (cortical) mice were transfected at DIV6–DIV8 using the calcium phosphate method adapted from[21], with the exception of the DIV3 live-cell imaging experiment, in which rat cortical neurons were transfected at DIV2. 2 μg of DNA or 1 μg of DNA from each DNA construct (double co-transfections) were used per coverslip; with the exception of co-transfections of GFP-tagged Rab proteins or Rip11 (WT and dominant negatives) with extracellular HA-tagged Nrxn1α, in which 0.75 μg and 1.25 μg of DNA was used for GFP-tagged and HA-Nrxn1α DNA constructs, respectively. Briefly, DNA plasmids were diluted in Tris-EDTA buffer (10 mM Tris-HCl and 2.5 mM EDTA, pH 7.3), followed by dropwise addition of $CaCl_2$ solution (2.5 M $CaCl_2$ in 10 mM HEPES, pH 7.2) to the plasmid DNA-containing solution to give a final concentration of 250 mM $CaCl_2$. This solution was subsequently added to an equal volume of HEPES-buffered solution (274 mM NaCl, 10 mM KCl, 1.4 mM Na_2HPO_4, 42 mM HEPES, pH 7.2) and vortexed gently for 3 s. This mixture, containing precipitated DNA, was then added dropwise to the coverslips in a 12-well plate, containing 250 μL of conditioned neuronal culture medium with kynurenic acid (2 mM), followed by 2 hr incubation in a 37 °C, 5% (vol/vol) CO_2/95% (vol/vol) air incubator. After 2 hr, the transfection solution was removed, after which 1 mL of conditioned neuronal culture medium with kynurenic acid (2 mM) slightly acidified with HCl (~5 mM final concentration) was added to each coverslip, and the plate was returned to a 37 °C, 5% (vol/vol) CO_2/95% (vol/vol) air incubator for 20 min. Finally, coverslips were then transferred to the original dish containing the conditioned culture medium in the 37 °C, 5% (vol/vol) CO_2/95% (vol/vol) air incubator to allow expression of the transfected constructs. Protein expression was typically for 24 hr (live-cell imaging and BFA assay) or 48 hr (immunocytochemistry experiments with fixed cells).

Immunocytochemistry

Cells were fixed for 10–15 min in 4% (wt/vol) sucrose and 4% (wt/vol) paraformaldehyde in PBS (PBS: 137 mM NaCl, 2.7 mM KCl, 1.8 mM KH_2PO_4 and 10 mM Na_2HPO_4, pH 7.4) at room temperature, and permeabilized with PBS + 0.25% (vol/vol) Triton X-100 for 5 min, at 4 °C. Neurons were then incubated in 10% (wt/vol) bovine serum albumin (BSA) in PBS for 1 hr at room temperature to block nonspecific staining, and incubated in appropriate primary antibodies diluted in 3% (wt/vol) BSA in PBS (overnight, 4 °C). After washing 3 times in PBS, cells were incubated with the secondary antibodies diluted in 3% (wt/vol) BSA in PBS (1 hr, room temperature). The coverslips were mounted using Prolong Gold Antifade mounting medium (Thermo Fisher Scientific, Cat #P36930).

In all immunocytochemistry experiments performed to determine the subcellular distribution of proteins of interest (Nrxns, SorCS1, Caspr2, L1, MAP2 or GluA2) the axonal compartment was labeled by using antibodies against Ankyrin-G, a marker of the axon initial segment (NeuroMab, Cat #73-146 or Santa Cruz Biotechnology, Cat #sc-31778), and the somatodendritic compartment was labeled by using an anti-MAP2 antibody (Abcam, Cat #ab5392).

Surface immunostaining of endogenous and exogenous extracellular HA-tagged Nrxn1α and exogenous HA-tagged Caspr2

For surface immunostaining of exogenous HA-Nrxn1α and HA-Caspr2, live mouse cortical and hippocampal neurons were incubated with rabbit anti-HA (1:1000 dilution; Sigma-Aldrich, Cat #H6908) diluted in conditioned neuronal culture medium for 15 min at room temperature. For surface immunostaining of endogenous HA-Nrxn1α live mouse cortical *Nrxn1α*$^{HA/HA}$ KI neurons were incubated with rabbit anti-HA (1:100 dilution; Cell Signaling Technology, Cat #3724) diluted in conditioned neuronal culture medium for 20 min at room temperature. Neurons were then fixed in 4% (wt/vol) sucrose and 4% (wt/vol) paraformaldehyde in PBS for 10 min at room temperature, followed by several washes in PBS and blocking in 10% (wt/vol) BSA in PBS for 1 hr at room temperature. Neurons were then incubated with anti-rabbit secondary antibody diluted in 3% (wt/vol) BSA in PBS (1 hr, room temperature). Following permeabilization, neurons were processed for immunocytochemistry as described above.

Surface immunostaining of extracellular myc-tagged L1

To allow surface immunostaining of myc-L1 (live labeling proved to be impossible), neurons were fixed first, followed by several washes and blocking, and then incubated with mouse anti-myc (1:1000 dilution; Santa Cruz Biotechnology, Cat #sc-40) diluted in 3% (wt/vol) BSA in PBS overnight at 4 °C. Subsequently, neurons were incubated with the respective secondary antibody for 1 hr at room temperature, and processed for immunocytochemistry as described above.

Antibody pulse-chase experiments

Cultured living neurons were incubated at room temperature for 10 min in the presence of a high concentration (1:250) of a mouse anti-HA antibody (Covance, Cat #MMS-101P), against extracellular HA-tagged Nrxn1α and SorCS1, diluted in conditioned medium. Neurons were then washed with pre-warmed PBS at 37 °C to remove the unbound antibody, and were further incubated in antibody free conditioned medium in a 37 °C, 5% (vol/vol) CO_2/95% (vol/vol) air incubator (for different periods) to allow the internalization of antibody-bound receptors. After this incubation, neurons were fixed in 4% (wt/vol) sucrose and 4% (wt/vol) paraformaldehyde in PBS for 10 min at room temperature. Next, neurons were either exposed to a super-saturating concentration (1:300) of the first of two secondary antibodies, to label the primary antibody-bound surface pool of protein, and/or incubated overnight with Fab fragments anti-mouse [0.25 mg/mL (Santa Cruz Biotechnology, Cat #715-007-003) in 5% (wt/vol) BSA in PBS] to block all primary antibody-bound receptors that were not internalized and/or not labeled by the first secondary antibody. After permeabilization, cells were processed for immunocytochemistry as described above, and the pool of internalized receptors was labeled by incubation with the second secondary antibody (1:1000) for 1 hr at room temperature. This strategy allows differential labeling of cell surface and internalized pools of protein.

Brefeldin A (BFA) assay

Mouse cortical neurons expressing extracellular HA-tagged Nrxn1α for 4 hr were treated with 0.75 µg/mL brefeldin A (Sigma-Aldrich, Cat #B5936) added to the coverslips in a 12-well plate containing conditioned neuronal culture medium. After 16 hr of treatment, coverslips were washed twice in pre-warmed neuronal culture medium, transferred to their original dishes containing conditioned neuronal culture medium and fixed for 10 min in 4% (wt/vol) sucrose and

4% (wt/vol) paraformaldehyde in PBS at various intervals thereafter (1, 2, and 4 hr after BFA washout). Internal and surface pools of Nrxn1α were then differentially labeled. First, neurons were blocked in 10% (wt/vol) bovine serum albumin (BSA) in PBS for 1 hr at room temperature and incubated (overnight, 4 °C) with mouse anti-HA (1/1000) (Covance, Cat #MMS-101P) diluted in 3% (wt/vol) BSA in PBS. After, several washes neurons were incubated with super-saturating concentration (1/300) of anti-mouse secondary antibody diluted in 3% (wt/vol) BSA in PBS 1 hr at room temperature. Remaining unlabelled primary antibody-bound surface HA-Nrxn1α was blocked with overnight incubation with Fab fragments anti-mouse [0.13 mg/mL (Santa Cruz Biotechnology, Cat #715-007-003) in 5% (wt/vol) BSA in PBS]. After permeabilization, cells were processed for immunocytochemistry as described above to label the axonal and somatodendritic compartments and the pool of internal HA-Nrxn1α, labeled with an incubation with the same anti-HA (1/1000) primary antibody, followed by incubation with the respective secondary antibodies for 1 hr at room temperature. This strategy allows differential labeling of cell surface and internal pools of HA-Nrxn1α.

Dynasore treatment

Mouse cortical or hippocampal neurons expressing extracellular HA-tagged Nrxn1α for 30 hr were either treated with 20 μM Dynasore (Sigma-Aldrich, Cat #D7693) or DMSO, added to the coverslips in a 12-well plate containing conditioned neuronal culture medium, for 18 hr. Afterwards, surface HA-Nrxn1α was labeled in live neurons as described above.

TTX and PTX treatment

DIV6–DIV8 mouse cortical neurons either immediately after transfection with HA-Nrxn1α or untransfected were treated for 48 hr (refreshed after 24 hr) with 1 μM tetrodotoxin (TTX) (Tocris, Cat #1069) or 30 μM picrotoxin (PTX) (Tocris, Cat #1128) dissolved in dimethyl sulfoxide (DMSO). Neurons were then processed for immunocytochemistry as described above.

Image Analysis and Quantification

All images obtained from immunocytochemistry experiments in fixed cells were captured on a Leica SP8 laser-scanning confocal microscope (Leica Micro-systems). The same confocal acquisition settings were applied to all images taken from a single experiment. Parameters were adjusted so that the pixel intensities were below saturation. Fiji analysis software was used for quantitative imaging analysis. Z-stacked images were converted to maximal intensity projections and thresholded using constant settings per experiment.

Quantification of axonal and dendritic immunofluorescence intensity and ratio of axonal/dendritic immunofluorescence intensity

Fluorescence intensity was measured as the sum of integrated intensity in representative portions of axons and dendrites using Ankyrin-G and MAP2 as guides, respectively. Axonal and dendritic intensities were divided by neuritic length and total intensity (axonal + dendritic) (‘*Relative Axonal Intensity’* and ‘*Relative Dendritic Intensity’*) to adjust measurements across cells with varying expression levels (exogenous expression). The A/D ratio was then calculated by dividing the values of axonal and dendritic intensities obtained for every cell (‘*Axonal/Dendritic Intensity’*). A uniformly distributed protein yields an A/D ratio of around 1. A preferentially dendritically localized protein yields an A/D ratio < 1, whereas a preferentially axonally localized protein yields an A/D ratio > 1. To quantify the fluorescence

intensity of endogenous Nrxns, axonal and dendritic intensities were not normalized to the total intensity (‘*Axonal Intensity’* and ‘*Dendritic Intensity’*).

Classical polarity index measurement

In some cases polarization of cargo was determined by using the classical polarity index originally described by[22,23]. This index does not provide a direct measurement of the axonal and dendritic fluorescent intensities, but it allows a quick estimation of the compartmentalized polarization of proteins of interest. One-pixel-wide lines were traced along three dendrites and representative portions of the axon, using MAP2 and Ankyrin-G as guides, in non-thresholded images. The mean intensities (dendritic was averaged from three dendrites) were used to calculate the dendrite:axon (D:A) ‘*Polarity Index’*. D:A = 1, uniform staining; D:A < 1, preferential axonal staining; D:A > 1, preferential dendritic staining.

BFA-assay and long-term live-cell imaging

Fluorescence intensity was measured as the sum of integrated intensity in representative portions of axons and dendrites (using Ankyrin-G and MAP2 as guides); and cell bodies. In the case of long-term live-cell imaging, axonal and dendritic intensities were divided by neuritic length, and somatic intensities by somatic area (‘*Nrxn Intensity’* or ‘*TfR Intensity’*). In case of the BFA-assay, axonal and dendritic intensities were divided by neuritic length and total intensity [surface (axonal and dendritic) + internal (axonal and dendritic)] (*‘Relative Axonal Intensity’* and ‘*Relative Dendritic Intensity’*).

Antibody pulse-chase experiments

Fluorescence intensity was measured as the sum of integrated intensity in representative portions of axons and dendrites using Ankyrin-G and MAP2 as guides, respectively. Intensities of internalized SorCS1 and Nrxn were divided by neuritic length and by the total intensity (surface + internal) (‘*Relative Intensity of Internalized Nrxn’ or ‘SorCS’*) or by the total internalized intensity (axonal + dendritic) (‘*Relative Intensity of Internalized Nrxn’).* Intensities of surface SorCS1 were also divided by neuritic length and by the total intensity (surface + internal) (‘*Relative Intensity of Surface SorCS1’*).

Manders coefficient

Manders coefficient was measured by using the Fiji plugin JACoP[24]. Manders coefficient measures the proportion of the signal from channel ‘a’ that coincides with the signal in channel ‘b’ over the total intensity of ‘a’ – M1 coefficient[25]. For our measurements internalized Nrxn was defined as channel ‘a’ and endosomal markers (Figure S3) or SorCS1 (Figure S6) as channel ‘b’; and Rip11 as channel ‘a’ and SorCS1 as channel ‘b’ (Figure 6).

Colocalization of internalized Nrxn with endosomal markers in Sorcs1 KO cells

The colocalization of internalized Nrxn with endosomal markers was evaluated by measuring the density of double-positive puncta for internalized Nrxn and endosomes and by measuring the intensity of Nrxn present in these puncta. Fluorescence intensity was measured as the sum of mean intensity of internalized Nrxn puncta (defined as 0.02 μm^2-infinite) in representative portions of axons and dendrites (using Ankyrin-G and MAP2 as guides), colocalizing with endosomal markers. Intensities of internalized Nrxn were divided by neuritic length (‘*Nrxn Intensity in Double Positive*

Puncta'). Density of internalized Nrxn puncta (defined as 0.02 μm^2-infinite), colocalizing with endosomal markers, was also divided by neuritic length ('*Double Positive Puncta Density'*).

Live-Cell Imaging

For live-cell imaging of fluorescently tagged Nrxn1α- and TfR-positive vesicles, neurons were transfected with a bicistronic expression plasmid encoding Streptavidin-KDEL and SBP-GFP-Nrxn1α or Streptavidin-KDEL and TfR-SBP-GFP, respectively, using the RUSH system[6]. After transfection neurons were maintained in Neurobasal medium without B27 supplement, because the presence of D-biotin in B27 interferes with the RUSH system, or in Neurobasal medium supplemented with N-2 supplement (Thermo Fisher Scientific, Cat #P36930), which lacks D-biotin. Live-cell imaging was performed at room temperature (~20°C) in imaging medium (119 mM NaCl, 5 mM KCl, 2 mM CaCl2, 2 mM MgCl2, 30 mM glucose, and 10 mM Hepes, pH 7.4). For long-term live-cell imaging experiments DIV8–DIV10 or DIV3 rat cortical neurons, after 24–31 hr or 25–29 hr of protein expression, respectively, were imaged on a Nikon Eclipse Ti A1R confocal microscope. Images were collected with a 40x oil objective (1.3 NA; Nikon). Focal drift during the experiment was avoided by using the perfect focus system feature of the Nikon system. Laser intensities were kept as low as possible. Time-lapses lasted for 2,5 hr and frames were acquired as z-stacks every 5 min. Synchronous release of Nrxn1α or TfR was induced by application of 40 μM D-biotin (Sigma-Aldrich, Cat #B4501) 10 min after the beginning of the imaging session. Protein synthesis was inhibited by including 20 μg/mL cycloheximide (Sigma-Aldrich, Cat #C4859) in the imaging medium. For short-term live-cell imaging experiments DIV8–DIV10 rat cortical neurons expressing Streptavidin-KDEL and SBP-GFP-Nrxn1α, 21–30 hr after protein expression, were imaged on a Nikon spinning-disk confocal microscope equipped with a 60x oil objective (1.4 NA; Nikon). Time-lapses were performed by sequential capture of 200-ms images of SBP-GFP-Nrxn1α every second for 60–120 s. Focal drift during the experiment was corrected automatically using the autofocus feature of the Nikon system. Neurons were imaged either for 20–34 min or 1–2 hr after exposure to 40 μM D-biotin. In both experiments, a single image of live-stained pan-Neurofascin was taken at the beginning of every imaging session.

Live labeling of the axon initial segment (AIS)

Before every live-cell imaging experiment primary rat cortical cultured neurons were live-labeled with an anti-pan-Neurofascin antibody (NeuroMab, Cat #75-172) to distinguish the axon from the dendrites. Live-cell imaging experiments were performed with rat cortical neurons because live-labeling of the AIS with the anti-pan-Neurofascin antibody did not work in mouse cultured neurons. Briefly, coverslips with neurons were quickly rinsed in pre-warmed neuronal culture medium. Neurons were incubated with anti-pan-Neurofascin antibody (1/500) diluted in conditioned neuronal culture medium for 10 min in a 37 °C, 5% (vol/vol) CO_2/95% (vol/vol) air incubator. Coverslips were then quickly washed twice with pre-warmed neuronal culture medium. Finally, neurons were incubated with an Alexa-555 anti-mouse (1/400) (Invitrogen, Cat #A31570) secondary antibody diluted in conditioned neuronal culture medium and incubated for 10 min in a 37 °C, 5% (vol/vol) CO_2/95% (vol/vol) air incubator. Neurons were quickly rinsed twice with pre-warmed neuronal culture medium and used for live-cell imaging experiments.

Analysis of Nrxn1α- and TfR-positive vesicle transport

Dendrites and axon were imaged from the same neuron using spinning disk confocal microscopy. Time-lapses were performed by sequential capture of 200-ms images every second for 60–120 s. Acquisitions were analyzed using an

Igor-based software developed by Pieter Vanden Berghe and Valérie Van Steenbergen (Lab. for Enteric NeuroScience and Cell Imaging Core, KU Leuven). Kymographs were created using a segmented line along the axon/dendrite (one dendrite was analysed per cell) from the soma towards the neurite tip, so that anterograde movement occurred from left to right. On the kymographs, single vesicle movement episodes were distinguished as tilted straight lines. Single vesicle pauses were distinguished as straight lines. The number of moving anterograde/retrograde particles in the dendrite and axon was determined manually by drawing lines on top of the trajectories of single particles obtained from the kymographs. Vesicles were defined as motile when showing net displacement of 2 ≥ µm.

Biochemistry

Detection of HA-tagged endogenous SorCS1 and Nrxn1α

Adult brains (*Sorcs1*$^{HA/HA}$, P60 total brain) or (*Nrxn1α*$^{HA/HA}$, three-month-old cortices) from wildtype (+/+), heterozygous (+/Tg) and homozygous (Tg/Tg) KI mice were dissected, snap frozen and stored at -80 °C. The tissue was homogenized in homogenization buffer (20 mM HEPES, pH 7.4; 320 mM sucrose, 5 mM EDTA) supplemented with protease inhibitors (Roche, Cat #11697498001) using a glass Dounce homogenizer. Homogenates were spun at 3000 x g for 15 min at 4 °C. Supernatants were collected and protein quantification was performed with Bio-Rad protein Assay (Cat #500-0006). Samples were analyzed by western blot using a mouse anti-HA antibody (Covance, Cat #MMS-101P; *Sorcs1*$^{HA/HA}$ KI) or a rabbit anti-HA antibody (Cell Signaling Technology, Cat #3724; *Nrxn1α*$^{HA/HA}$ KI). A total protein stain (Ponceau) was used to assess equal protein loading and transfer to nitrocellulose membrane.

Immunoprecipitation of HA-tagged endogenous SorCS1

Cortices from adult *Sorcs1*$^{HA/HA}$ KI mouse brains were dissected and homogenized in homogenization buffer (50 mM HEPES pH 7.4, 100 mM NaCl, 2 mM $CaCl_2$, 2.5 mM $MgCl_2$) supplemented with protease inhibitors (Roche, Cat #11697498001) using a Dounce homogenizer. Cortical homogenates were extracted with 1% CHAPSO (VWR, Cat #A1100.0005) in homogenization buffer while rotating end-over-end for 2 hr at 4°C and centrifuged at 100,000 x g for 1 hr at 4°C to pellet insoluble material. Supernatants were precleared by adding 100 µL of Protein-G agarose beads (Thermo Fisher Scientific, Cat #22852BR) and rotating for 1 hr at 4°C, then incubated with 5 µg of mouse IgG or 50 µL of anti-HA magnetic beads (Thermo Fisher Scientific, Cat #88836) and rotated end-over-end overnight at 4°C. 60 µL of Protein-G agarose beads were added to the IgG control sample and rotated for 1 hr at 4°C, followed by three washes in cold extraction buffer and once in PBS. Anti-HA magnetic beads were washed according to the manufacturer's protocol using a magnetic stand. Protein-G agarose beads and anti-HA magnetic beads were heated for 15 minutes at 40°C in 50 µL 2X sample buffer and analysed by western blotting.

Lentivirus Production

Second generation VSV.G pseudotyped lentiviruses were produced as described [11,26]. HEK293T cells were transfected with control (mCherry) or Cre-T2A-mCherry-containing pFUGW vector plasmids and helper plasmids PAX2 and VSVG using Fugene6 (Promega, Cat #E2691). Supernatant was collected 65 hr after transfection and filtered through a 0.45 µm filter (Thermo Fisher Scientific, Cat #723-2545), aliquoted and stored at -80 °C.

Electrophysiology

Neurons were recorded on DIV11–DIV16. The patch pipette solution contained (in mM): 136 KCl, 18 HEPES, 4 Na-ATP, 4.6 $MgCl_2$, 4 K_2-ATP, 15 Creatine Phosphate, 1 EGTA and 50 U/ml Phospocreatine Kinase (300 mOsm, pH 7.30). The external medium used contained the following components (in mM): 140 NaCl, 2.4 KCl, 4 $CaCl_2$, 4 $MgCl_2$, 10 HEPES, 10 Glucose (300 mOsm, pH 7.30). Cells were whole-cell voltage clamped at −70 mV with a double EPC-10 amplifier (HEKA Elektronik) under control of Patchmaster v2x32 software (HEKA Elektronik). Currents were low-pass filtered at 3 kHz and stored at 20 kHz. Patch pipettes were pulled from borosilicate glass using a multi-step puller (P-1000; Sutter Instruments). Pipette resistance ranged from 3 to 5 MΩ. The series resistance was compensated to ~75%. Only cells with series resistances below 15 MΩ were included for analysis. All recordings were made at room temperature. Spontaneous glutamatergic release was (sEPSC) was recorded at -70 mV. Evoked release was induced using brief depolarization of the cell soma (from 70 to 0 mV for 1 ms) to initiate action potential-dependent glutamatergic release (eEPSCs). A fast local multi-barrel perfusion system (Warner SF-77B, Warner Instruments) was used determine the RRP size using external recording solution containing 500 mM sucrose. A custom analysis procedure in Igor Pro (Wavemetrics Inc.) was used for offline analysis of evoked and sucrose responses. Spontaneous events were detected using Mini Analysis program (Synaptosoft).

Statistical Analysis

The results are shown as average or as average ± s.e.m., with n referring to the number of analyzed neurons for each group. For most experiments at least 3 independent cultures were included for analysis. Datasets were tested either using Mann-Whitney *U* test or Kruskal-Wallis test by Dunn's multiple comparisons test. Statistical testing was performed using GraphPad Prism (GraphPad Software). In all instances, statistical significance was defined as follows: n.s. - not significant ($p > 0.05$), * $p< 0.05$, ** $p < 0.01$, *** $p < 0.001$.

SUPPLEMENTARY REFERENCES

1. Gokce, O. & Sudhof, T. C. Membrane-Tethered Monomeric Neurexin LNS-Domain Triggers Synapse Formation. *J. Neurosci.* **33**, 14617–14628 (2013).

2. Zhang, C. *et al.* Neurexins Physically and Functionally Interact with GABAA Receptors. *Neuron* **66**, 403–416 (2010).

3. Ehlers, M. D. Dendritic trafficking for neuronal growth and plasticity. *Biochem. Soc. Trans.* **41**, 1365–1382 (2013).

4. Schmidt, M. R. & Haucke, V. Recycling endosomes in neuronal membrane traffic. *Biol. Cell* **99**, 333–342 (2007).

5. Moulder, K. L. Reluctant Vesicles Contribute to the Total Readily Releasable Pool in Glutamatergic Hippocampal Neurons. *J. Neurosci.* **25**, 3842–3850 (2005).

6. Boncompain, G. *et al.* Synchronization of secretory protein traffic in populations of cells. *Nat. Methods* **9**, 493–498 (2012).

7. Farías, G. G., Guardia, C. M., Britt, D. J., Guo, X. & Bonifacino, J. S. Sorting of Dendritic and Axonal Vesicles at the Pre-axonal Exclusion Zone. *Cell Rep.* **13**, 1221–1232 (2015).

8. Taniguchi, H. *et al.* Silencing of Neuroligin Function by Postsynaptic Neurexins. *J. Neurosci.* **27**, 2815–2824 (2007).

9. Lane, R. F. *et al.* Diabetes-Associated SorCS1 Regulates Alzheimer's Amyloid-Metabolism: Evidence for Involvement of SorL1 and the Retromer Complex. *J. Neurosci.* **30**, 13110–13115 (2010).

10. de Wit, J. *et al.* LRRTM2 Interacts with Neurexin1 and Regulates Excitatory Synapse Formation. *Neuron* **64**, 799–806 (2009).

11. Dittgen, T. *et al.* Lentivirus-based genetic manipulations of cortical neurons and their optical and electrophysiological monitoring in vivo. *Proc. Natl. Acad. Sci.* **101**, 18206–18211 (2004).

12. Meyers, J. M. & Prekeris, R. Formation of Mutually Exclusive Rab11 Complexes with Members of the Family of Rab11-interacting Proteins Regulates Rab11 Endocytic Targeting and Function. *J. Biol. Chem.* **277**, 49003–49010 (2002).

13. Gil, O. D. *et al.* Ankyrin binding mediates L1CAM interactions with static components of the cytoskeleton and inhibits retrograde movement of L1CAM on the cell surface. *J. Cell Biol.* **162**, 719–730 (2003).

14. Bel, C., Oguievetskaia, K., Pitaval, C., Goutebroze, L. & Faivre-Sarrailh, C. Axonal targeting of Caspr2 in hippocampal neurons via selective somatodendritic endocytosis. *J. Cell Sci.* **122**, 3403–3413 (2009).

15. Woo, J. *et al.* Trans-synaptic adhesion between NGL-3 and LAR regulates the formation of excitatory synapses. *Nat. Neurosci.* **12**, 428–437 (2009).

16. Damke, H., Baba, T., Warnock, D. E. & Schmid, S. L. Induction of mutant dynamin specifically blocks endocytic coated vesicle formation. *J. Cell Biol.* **127**, 915–934 (1994).

17. Pregno, G. *et al.* Differential regulation of neurexin at glutamatergic and GABAergic synapses. *Front. Cell. Neurosci.* **7**, (2013).

18. Prekeris, R., Klumperman, J. & Scheller, R. H. A Rab11/Rip11 protein complex regulates apical membrane trafficking via recycling endosomes. *Mol. Cell* **6**, 1437–1448 (2000).

19. Kaech, S. & Banker, G. Culturing hippocampal neurons. *Nat. Protoc.* **1**, 2406–2415 (2006).

20. Bekkers, J. M. & Stevens, C. F. Excitatory and inhibitory autaptic currents in isolated hippocampal neurons maintained in cell culture. *Proc. Natl. Acad. Sci. U. S. A.* **88**, 7834–7838 (1991).

21. Jiang, M., Deng, L. & Chen, G. High Ca2+-phosphate transfection efficiency enables single neuron gene analysis. *Gene Ther.* **11**, 1303–1311 (2004).

22. Sampo, B., Kaech, S., Kunz, S. & Banker, G. Two Distinct Mechanisms Target Membrane Proteins to the Axonal Surface. *Neuron* **37**, 611–624 (2003).

23. Wisco, D. *et al.* Uncovering multiple axonal targeting pathways in hippocampal neurons. *J. Cell Biol.* **162**, 1317–1328 (2003).

24. Bolte, S. & Cordelières, F. P. A guided tour into subcellular colocalization analysis in light microscopy. *J. Microsc.* **224**, 213–232 (2006).

25. Manders, E. M. M., Verbeek, F. J. & Aten, J. A. Measurement of co-localization of objects in dual-colour confocal images. *J. Microsc.* **169**, 375–382 (1993).

26. Kutner, R. H., Zhang, X.-Y. & Reiser, J. Production, concentration and titration of pseudotyped HIV-1-based lentiviral vectors. *Nat. Protoc.* **4**, 495–505 (2009).

SUPPLEMENTARY VIDEOS and LEGENDS

Supplementary Movie 1

DIV8 WT rat cortical neuron co-expressing the ER-hook (Streptavidin-KDEL) and SBP-GFP-Nrxn1α (grayscale, inverted for clarity) and live-stained for the AIS marker Neurofascin to label the axon. Biotin was added 10 min after the beginning of the imaging session. Cell was recorded every 5 min for 2,5 hr. The axon is indicated. Frame rate: 2 fps.

Supplementary Movie 2

DIV9 WT rat cortical neuron co-expressing the ER-hook (Streptavidin-KDEL) and TfR-SBP-GFP (grayscale, inverted for clarity) and live-stained for the AIS marker Neurofascin to label the axon. Biotin was added 10 min after the beginning of the imaging session. Cell was recorded every 5 min for 2,5 hr. The axon is indicated. Frame rate: 2 fps.

Supplementary Movie 3

DIV10 WT rat cortical neuron co-expressing the ER-hook (Streptavidin-KDEL) and SBP-GFP-Nrxn1α (grayscale, inverted for clarity) and live-stained for the AIS marker Neurofascin to label the axon. Cell was recorded every second for 30 s. The axon is indicated. Frame rate: 4 fps.

Supplementary Movie 4

DIV3 WT rat cortical neuron co-expressing the ER-hook (Streptavidin-KDEL) and SBP-GFP-Nrxn1α (grayscale, inverted for clarity) and live-stained for the AIS marker Neurofascin to label the axon. Biotin was added 10 min after the beginning of the imaging session. Cell was recorded every 5 min for 2,5 hr. The axon is indicated. Frame rate: 2 fps.

Supplementary Movie 5

DIV9 WT rat cortical neuron co-expressing the ER-hook (Streptavidin-KDEL) and SBP-GFP-Nrxn1α (grayscale, inverted for clarity) and live-stained for the AIS marker Neurofascin to label the axon. Cell was incubated with biotin for 22 min and then recorded every second for 120 s. The axon is indicated. Frame rate: 4 fps.

Supplementary Movie 6

DIV10 WT rat cortical neuron co-expressing the ER-hook (Streptavidin-KDEL) and SBP-GFP-Nrxn1α (grayscale, inverted for clarity) and live-stained for the AIS marker Neurofascin to label the axon. Cell was incubated with biotin for 1 hr and 55 min and then recorded every second for 120 s. The axon is indicated. Frame rate: 4 fps.